NOAA Technical Memorandum OAR PMEL-131

Assessment of Potential Tsunami Impact for Pearl Harbor, Hawaii

L. Tang[1], C. Chamberlin[1], E. Tolkova[1], M. Spillane[1], V.V. Titov[1], E.N. Bernard[2], and H.O. Mofjeld[2]

[1]Joint Institute for the Study of the Atmosphere and Ocean
University of Washington
Box 351640
Seattle, WA 98195

[2]Pacific Marine Environmental Laboratory
7600 Sand Point Way NE
Seattle, WA 98115-6349, USA

August 2006

Contribution 2984 from NOAA/Pacific Marine Environmental Laboratory

NOTICE

Mention of a commercial company or product does not constitute an endorsement by NOAA/OAR. Use of information from this publication concerning proprietary products or the tests of such products for publicity or advertising purposes is not authorized.

Contribution No. 2984 from NOAA/Pacific Marine Environmental Laboratory

For sale by the National Technical Information Service, 5285 Port Royal Road
Springfield, VA 22161

Contents

List of Figures

Executive Summary

It is proposed that the NOAA/Pacific Region Center facility (including the Pacific Tsunami Warning Center) be moved to a new site at Ford Island that is located inside Pearl Harbor, Hawaii on the Island of Oahu. One issue to consider in evaluating the new site is the likelihood of tsunami inundation. To address this issue, the NOAA/PMEL/Center for Tsunami Research has carried out a detailed tsunami modeling study for the Oahu area. The study focused on the distant tsunami hazard because historical data do not reflect a local tsunami hazard over the expected life of the NOAA building (60 years). This study was based on available information on past distant tsunamis striking Pearl Harbor, as well as a scenario of distant tsunamis from the major subduction zone sources throughout the Pacific region.

The tsunami model used the best available data on water depths and land elevations, including any recent changes in either. This was necessary because the behavior of tsunamis can be very sensitive to even small variations of the water depths nearshore, the location of the shoreline, and the land elevations within any possible inundation zones. The numerical tsunami inundation model used in the study has been thoroughly validated and is the basis for the new U.S. tsunami forecast system being implemented at the NOAA Tsunami Warning Centers.

The results of the study show that none of the tsunamis observed in the past nor any of the 18 modeled scenario events—based on great subduction zone earthquakes—have caused inundation at the NOAA building site. The results from the scenarios evaluated indicated that the maximum rise in water levels anywhere at Ford Island for all considered sources was less than 1.5 m (5 ft) above mean high water level (MHW). The NOAA building site on Ford Island is located at +3.0 m above MHW.

Assessment of Potential Tsunami Impact for Pearl Harbor, Hawaii

L. Tang[1], C. Chamberlin[1], E. Tolkova[1], M. Spillane[1], V.V. Titov[1], E.N. Bernard[2], and H.O. Mofjeld[2]

Abstract. A 1/3 arc-second (10 m) high-resolution tsunami inundation model utilizing the 2D MOST model was developed for Pearl Harbor, Hawaii. The present study focuses on validating the model with historical tsunami water level records, identifying the worst-case scenario, and evaluating the potential impacts on Pearl Harbor. A secondary objective is to explore the effect of the changed Honolulu coastline on tsunami waves.

This study examined nine historical tsunamis, including four recent events with high quality measurements at DART buoys and tide gages, and five destructive tsunamis in Hawaiian history. The model tsunamis were in excellent agreement with the observations for the four recent events, as well as for the 1964 Alaska and 1946 Unimak tsunamis. The model also yielded reasonable comparisons for the 1952 Kamchatka, 1957 Andreanof, and 1960 Chile tsunamis. These comparisons provide validation references for the tsunami vulnerability study.

The NCTR's pre-computed propagation database provided the computed maximum wave amplitudes at a site offshore of Pearl Harbor from 804 synthetic tsunami sources around the Pacific Ocean. These data, combined with their directionalities, served as guidance for selecting 18 simulated 9.3 M_w tsunamis, one from each of the major subduction zones. An inundation test model with 1 arc-second (30 m) resolution was employed to quickly identify the worst-case scenario, which is then used in the high-resolution model. The comprehensive modeling results indicate that hazardous wave conditions are likely to be created in the study area by tsunamis originating from the Kamchatka, East Philippine, Japan, Alaska-Aleutian, South American, and Cascadia Subduction Zones. In particular, the Kamchatka scenario produces the most severe impact on the study site. The unit source NZKT B38, to the north of Tonga, has the maximum offshore amplitude from a single unit source.

Computed waveforms at 16 points in the study area were used to evaluate the potential impacts on Pearl Harbor. With a typical incident wave period of 24 min or less, the north shore of Ford Island experiences significantly smaller waves than the open coast. When the typical incident wave period reaches 48 min or more, a characteristic resonance with a period of around 96 min at Pearl Harbor is excited, resulting in similar maximum wave amplitudes both inside Pearl Harbor and on the open coast. Larger wave heights and higher velocities are found in the Entrance Channel, the West Loch, and the channel near Hospital Point. Model results show no inundation at the NOAA building site for any of the simulations, including the five historical destructive tsunamis and the worst-case scenario.

A 1960 digital elevation model based on historical nautical charts of the region was developed. Modeling results indicate that changes in the Honolulu coastline since 1940 have little effect on the waveforms in both Pearl Harbor and Honolulu Harbor.

1. Objective and Approach

This report describes the study of potential impact of distant-source tsunamis on Pearl Harbor, Hawaii to provide model results for evaluating the suitabil-

[1]Joint Institute for the Study of the Ocean and Atmosphere, Box 354235, University of Washington, Seattle, WA 98115-4235

[2]NOAA/Pacific Marine Environmental Laboratory, 7600 Sand Point Way NE, Seattle, WA 98115-6349

Table 1: Pacific Ocean unit sources (from north to south).

Abbr.	Subduction zone Name	Unit sources Line/zone	No./line
WASZ	West Aleutian Subduction Zone	AB	10
AASZ	Alaska-Aleutian Subduction Zone	AB	45
KKJT	Kuril-Kamchatka/Japan Trench Subduction Zone	AB	31
CCSZ	Cascadia Subduction Zone Sources	AB	10
RNSZ	Ryukus-Kyushu-Nankai Subduction Zone	AB	22
EPSZ	East Philippines Subduction Zone	AB	19
NGSZ	North New Guinea Subduction Zone	AB	15
YMIB	Yap-Marianas-Izu Bonin Subduction Zone	AB	39
CASZ	Central American Subduction Zone	AB	36
CESZ[1]	Columbia-Ecuador Subduction Zone	AB	18
MOSZ	Manus Ocean Convergence Boundary	AB	17
NBSV	New Britain-Solomons-Vanuatu Subduction Zone	AB	37
NZKT	New Zealand-Kermadec-Tonga Subduction Zone	AB	39
SASZ	South American Subduction Zone	AB	45
SCSZ1	South Chile Subduction Zone	AB	19
		Total:	**804**

[1] Recent addition to the database (• in Fig. 1).

ity of Ford Island as a site for the development of the Pacific Region Center facility. No local Hawaiian sources were considered in this study because no substantial Honolulu-area tsunamis that originated from local sources can be found in the historical record. This is in contrast to the Island of Hawaii, where local tsunamis have struck repeatedly. A search for local events was carried out using the NGDC Global Tsunami Database (2000 BC to present), which is based on the tsunami catalogs of Pararas-Carayannis and Calebaugh (1977) and Lander and Lockridge (1989). The search (over 1700–2006) revealed only three local tsunami events for Honolulu, and all of these were small (0.6 m in 1868, 0.03 m in 1951, and 0.1 m in 1975), even though 11 local tsunami events were reported for the Hawaii Islands during 1868–1989, 6 of which were generated by magnitude >6 earthquakes on the Island of Hawaii. Hence the historical documentation supports the focus on distant-source tsunamis. In addition, our study shows that all modeled tsunamis inside Pearl Harbor are smaller in amplitude than those of Honolulu Harbor.

The study uses the 2D finite-difference MOST model (Titov and González, 1997; Titov and Synolakis, 1998) based on nonlinear long-wave approximation. It evaluates the worst-case scenario assessment based on model validation of historical tsunamis. The NOAA Center for Tsunami Research (NCTR) has developed a linear propagation model database consisting of 804 tsunami sources at 15 subduction zones in the Pacific Ocean (Gica *et al.*, 2006). The database provides the boundary conditions, including wave amplitude and velocities, for a high-resolution Pearl Harbor inundation model. Figure 1 shows the calculation domain of the propagation database.

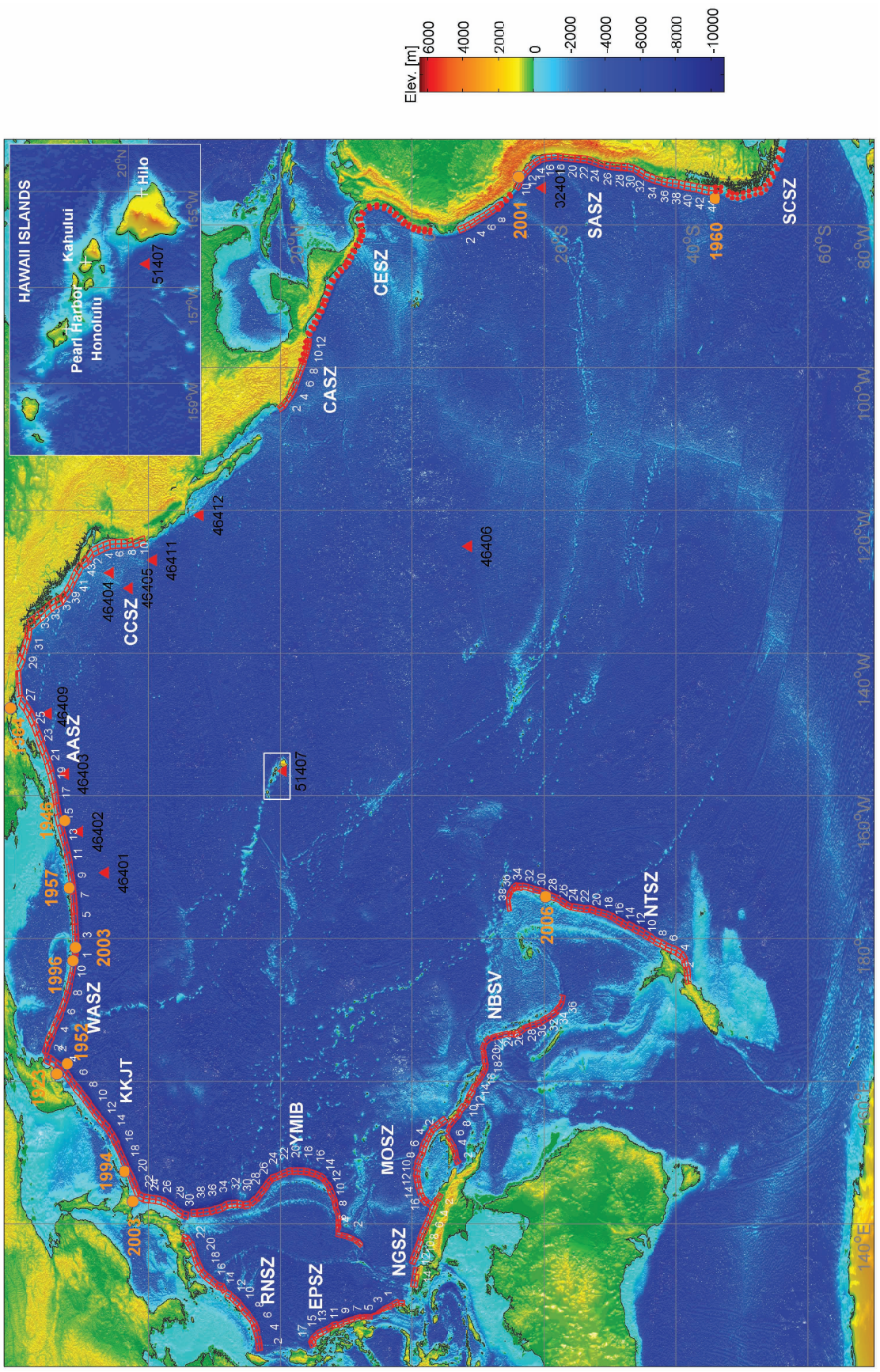

Figure 1: Computational domain of the propagation database. □/●, unit sources; ●, historical tsunamis; ▲, tsunameters (DARTs); Pearl Harbor (see inset).

2. Model Setup for Pearl Harbor

2.1 Study Area and Tsunami Data

The main Hawaiian Islands are the youngest and southernmost portion of the Hawaii Archipelago. From northwest to southeast, the islands form four natural geographic groups by shared channels and inter-island shelves, including (1) Ni'ihau, Ka'ula Rock, and Kauai (Kauai complex) (2) Oahu, (3) Molokai, Maui, Lanai, and Kaho'olawe (the Maui Complex), and (4) Hawaii (Smith, 1993). Pearl Harbor is located in the middle of Oahu's south shore and is the State's largest estuary.

The island of Oahu lies between Kauai, to the northwest, separated by the 115-km (72-mile) -wide Kauai Channel, and Molokai, to the southeast, by the 42-km (26-mile) -wide Kaiwi Channel. The island has a very angular shoreline, with a narrow insular shelf surrounding most of the island (Shepard *et al.*, 1950). On the southern side, the shelf terminates at a shallow depth of around 50 m with a very steep slope that extends out to 300 m. Then the seafloor slopes more gently down to the 500-m depth of the Kaiwi Channel. On the southeast side of the Kaiwi Channel, Penguin Bank is the most extensive shallow shelf area in the Hawaii Islands. The 50-m isobath reaches over 42 km (26 miles) eastward from the west end of Molokai.

The inundation study area covers half of the southern coastline of Oahu, including two natural harbors, Pearl Harbor and Honolulu Harbor. An aerial photo (Fig. 2) shows the location of the candidate site of the Pacific Region Center facility on the north shore of Ford Island, Pearl Harbor.

Hawaii has a long history of destructive distant-source tsunamis, which includes the 1946 Unimak, 1952 Kamchatka, 1957 Andreanof, 1960 Chile, and 1964 Alaska tsunamis. The Honolulu and Pearl Harbor tide stations recorded tsunamis from these events (Fig. 3). Established 1 January 1905 at Pier 4, Honolulu tide station has provided the most complete tsunami water-level data. It is the only station in Hawaii that recorded all of the five destructive tsunamis (Green, 1946; Zerbe, 1953; Berkman and Symons, 1964; Spaeth and Berkman, 1967). The Pearl Harbor tide station at Fort Kamehameha, Bishop Point, was installed on 27 July 1948 and removed on 24 March 1987 (http://tidesandcurrents.noaa.gov/). Data from this tide station is only available for the 1952 Kamchatka tsunami. Run-up records are available at seven locations (Walker, 2004). Inside Pearl Harbor, the 1946 tsunami generated 0.5 m (1.5 ft) run-up at the West Loch. The 1960 tsunami caused the most significant run-up, 3 m (9 ft) at both the open coast and Waikiki.

The local coastline and topography for three other locations, however, have been changed. The Honolulu coastline changed substantially from 1940 to 1966 with the construction of the Ala Wai Marina, Magic Island, and landfills in the port area around Sand Island. The 3.66-km (12,000-ft) Reef Runway of Honolulu International Airport in the shallow reef-lagoon between Honolulu Harbor and Pearl Harbor was built between 1973 and 1977. Simulation with prior bathymetry is necessary for the modeling of destructive historical tsunamis, because the behavior of tsunamis can be very sensitive to

Figure 2: An aerial photo of Pearl Harbor.

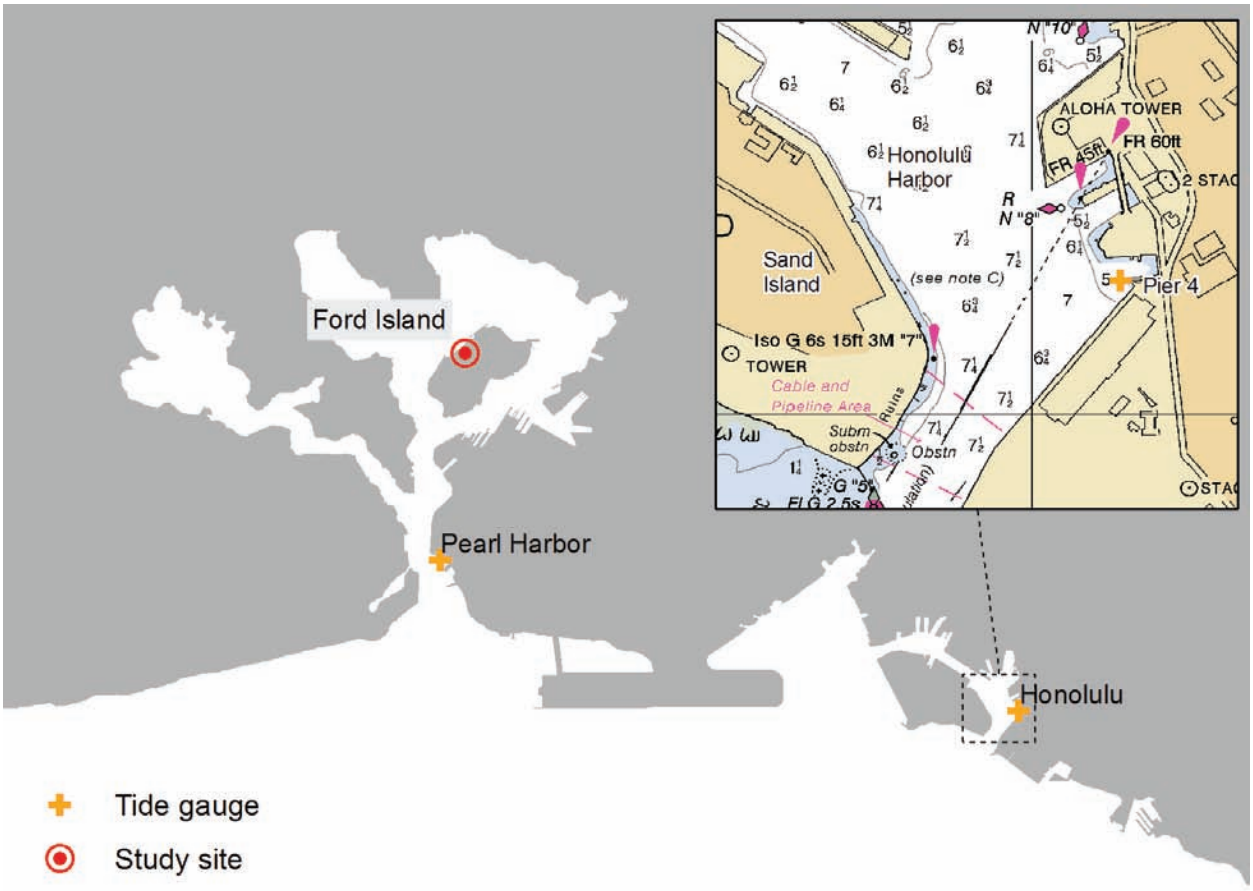

Figure 3: A map of Honolulu Harbor.

small variations in the water depths nearshore, the location of the shoreline, and the land elevations within any possible inundation zones. Four recent tsunamis from the 21st century are important in model validation and site assessment, since high quality DART and tide gage data are available and there is less ambiguity in the bathymetry and topography.

2.2 Bathymetry and Topography

Tsunami inundation modeling requires accurate bathymetry in coastal areas as well as high-resolution topography and bathymetry in the nearshore area. Digital elevation models (DEMs) were developed at medium resolution of 6 arc-second (180 m) covering all of the major Hawaiian Islands, and high resolution of 1/3 arc-second (10 m) covering the south Oahu area around Pearl Harbor. Both grids include topographic and bathymetric elevations. After compilation, the grids were resampled to produce the final modeling grids.

Table 2: Data sources used for grid development.

Data provider	Data type	Survey dates	Description
Bathymetric data			
Joint Airborne Lidar Bathymetry Technical Center of Excellence	Point	1999–2000	Nearshore bathymetry and topography from SHOALS airborne LIDAR. 1–5-m horizontal resolution.
Naval Oceanographic Office Fleet Survey Team	Point	2002	Pearl Harbor hydrographic survey. 8-m horizontal resolution.
Monterey Bay Aquarium Research Institute (MBARI)	Grid	1998	Multibeam bathymetric surveys. 10–30-m horizontal resolution.
USGS Pacific Seafloor Mapping Project	Grid	1998	Multibeam bathymetric surveys. 8-m horizontal resolution.
Japan Agency for Marine-Earth Science and Technology (JAMSTEC)	Grid	1998–2002	Multibeam bathymetric surveys. 150-m horizontal resolution. Multibeam tracklines at varying resolutions.
United States Navy	Point	2000	Multibeam surveys, south and west sides of Oahu.
U.S. Army Corps of Engineers, Honolulu District	Point	2000–2005	Digital echosounder surveys in USACE harbor project areas.
National Geophysical Data Center	Point	1968–1992	Bathymetric survey data. Multiple technologies, including lead line, digital echosounder, and multibeam.
NOAA Office of Coast Survey	Point	1979–2005	Bathymetric sounding data digitized from NOS nautical charts. Some points imported from Electronic Navigational Charts (ENCs).
Smith and Sandwell	Point	1997	2-min resolution bathymetry derived from satellite altimetry and ship tracklines.
USGS GLORIA	Point	1986–1988	Sidescan sonar bathymetric surveys in deep-water regions of Hawaii's EEZ.
Topographic data			
NOAA Coastal Services Center	Grid	2005	LIDAR topography.
USGS National Elevation Dataset	Grid	Varies	10-m horizontal resolution topographic data derived from USGS DEMs.

2.2.1 Data sources

The source grids were compiled from several data sources; Fig. 4 shows the spatial extent of each data source used. Table 2 is a summary of the data sources; in general, the data sources listed first superseded the sources listed later when they overlapped. The superseded datasets were used for comparison and verification.

High-resolution, recent topographic LIDAR data was available for the area of interest around Pearl Harbor. SHOALS bathymetric LIDAR data were used in nearshore areas around several islands, providing excellent coverage of reef and shoreline regions.

High-resolution gridded datasets derived from multibeam surveys are available for many parts of the archipelago, and were used wherever available.

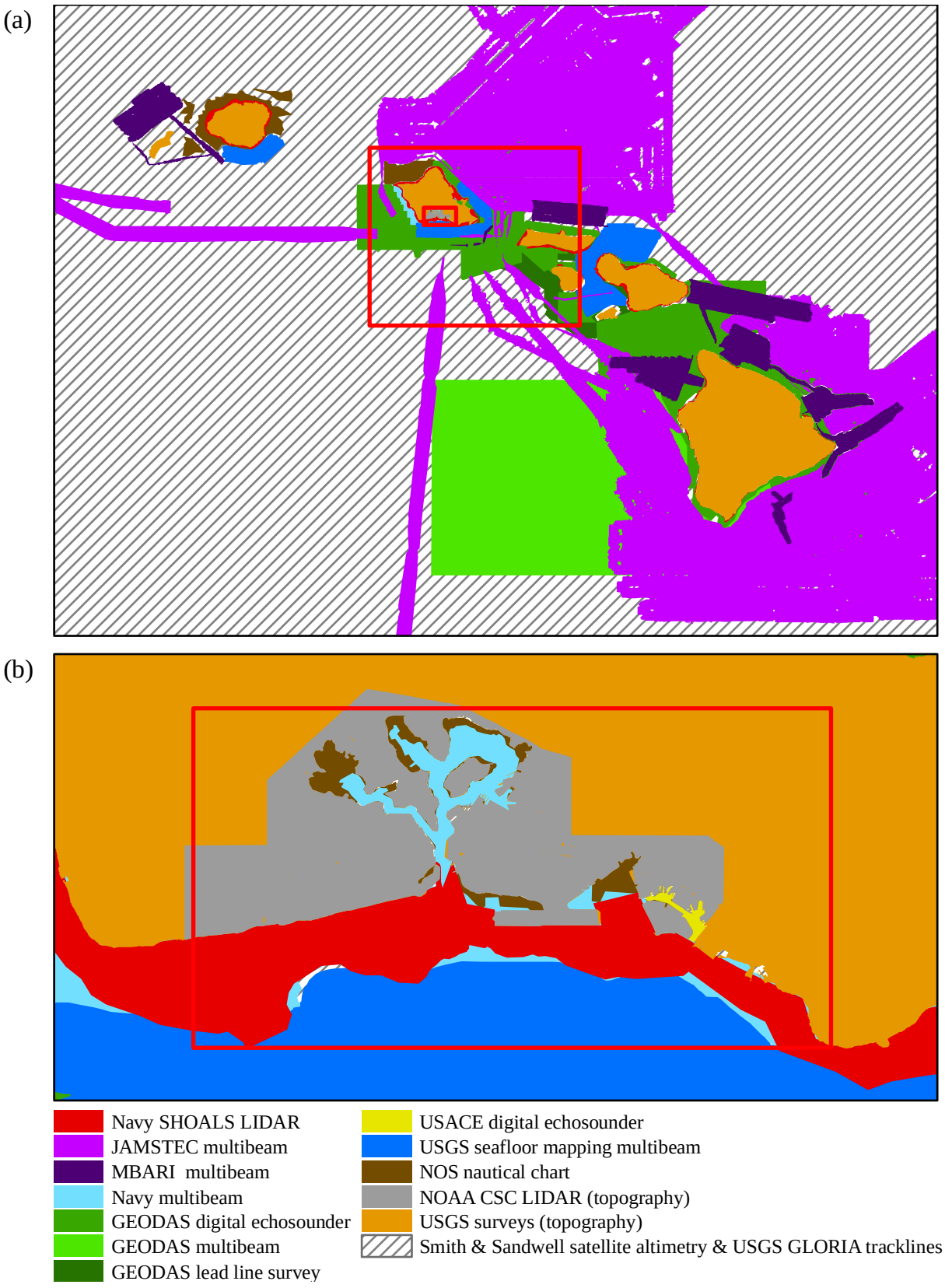

Figure 4: Bathymetric and topographic data source overview.

In deep water where high-resolution multibeam data were not available, the grid was developed by interpolation of a combination of USGS GLORIA surveys and the Smith and Sandwell 2-min (about 3.6 km in Hawaii) global seafloor dataset. These datasets were edited to remove individual points substantially different from nearby data.

Source details for the datasets incorporated into the model grids:

- Joint Airborne Lidar Bathymetry Technical Center of Expertise (JALBTCX), U.S. Army Corps of Engineers, Mobile District. Online reference: `http://shoals.sam.usace.army.mil/hawaii/pages/Hawaii\_Data.htm`.
- Naval Oceanographic Office Fleet Survey Team, Hydrographic Survey of Pearl Harbor, May 16 to June 20, 2002.
- Monterey Bay Aquarium Research Institute (MBARI) Hawaii Multibeam Survey, Version 1. Online reference: `http://www.mbari.org/data/mapping/hawaii/`.
- USGS Pacific Seafloor Mapping Project. Online reference: `http://walrus.wr.usgs.gov/pacmaps/data.html`.
- Japan Agency for Marine-Earth Science and Technology (JAMSTEC) 1998–1999 multibeam bathymetric surveys. Published in: Takahashi, E. *et al.*, eds. (2002): *Hawaiian Volcanoes: Deep Underwater Perspectives*. American Geophysical Union Monograph 128. JAMSTEC trackline data was recorded by the R/V *Mirai* during transits near Hawaii in 1999 and 2002. Online reference: `http://www.jamstec.go.jp/mirai/index\_eng.html`.
- United States Army Corps of Engineers (USACE), Honolulu District. Online reference: `http://www.poh.usace.army.mil/`.
- NOAA National Geophysical Data Center (NGDC). Online reference: `http://www.ngdc.noaa.gov/mgg/gdas/gd\_sys.html`.
- NOAA Office of Coast Survey. Sounding points were digitized from NOS nautical charts 19347, 19358, 19359, 19364, 19366, 19342, 19381, and 19324. Sounding data from electronic chart (ENC) 19357 were used. This data was included in relatively shallow regions where other data sources were sparse or unavailable, to fill small gaps between other data sources, and as quality control for other sources.
- NOAA Coastal Services Center Topographic Change Mapping Project, 2005 Oahu/Maui LIDAR mapping. Processed to bare earth and interpolated to 10 m gridded data by NOAA CSC. Online reference: `http://ekman.csc.noaa.gov/TCM/`.
- Smith, W.H.F., and D.T. Sandwell, Global seafloor topography from satellite altimetry and ship depth soundings, *Science, 277*, 1957–1962, 26 September 1997. Online reference: `http://topex.ucsd.edu/WWW\_html/mar\_topo.html`.
- USGS Geological Long-Range Inclined Asdic (GLORIA) surveys. Online reference: `http://walrus.wr.usgs.gov/infobank/`.

- USGS National Elevation Dataset. Online reference: `http://seamless.usgs.gov/`.

2.2.2 Grid compilation process

Raw data sources were imported to ESRI ArcGIS-compatible file formats. Data values were converted, where necessary, to the WGS84 horizontal geodetic datum. In the point datasets, single sounding points that differed substantially from neighboring data were removed. Gridded datasets were checked for extreme values by examination of contour lines and, where available, by comparison between multiple data sources.

All selected input datasets were converted to the mean high water (MHW) vertical datum, when necessary, using offsets on the National Ocean Service tidal benchmark datasheet for the Honolulu tide station.

To compile the multiple data sources into a single grid, subsets of the source data were created in the priority order described above. A triangulated irregular network (TIN) was created from the vector point. Also added to the TIN were points taken from the edges of the gridded data regions to ensure a smooth interpolated transition between areas with different data sources. This TIN was linearly interpolated using ArcGIS 3D Analyst to produce intermediate $1/3''$ arc-second (10 m) and 6 arc-second (180 m) raster grids. The gridded datasets were then bilinearly resampled to these resolutions and overlaid on the intermediate grids.

2.2.3 Historical comparison grid

In order to properly compare historical tsunami records with model results, a digital elevation model (DEM) matching the topography and bathymetry to that appropriate to the date of the tsunami event was required. We selected 1960 as the date for historical DEM development, since the 1960 Chile tsunami had the highest run-up records in the study area, and because of the availability of the historical maps prior to it.

The southern shore of Oahu between Pearl Harbor and Honolulu underwent substantial change between 1960 and 2006. The largest change was the construction in the mid-1970s of a new runway for Honolulu International Airport over a former reef area and seaplane landing strip. Several smaller areas in the Honolulu Harbor and Waikiki areas were also filled beginning in the 1960s.

To construct the 1960 DEM, historical nautical charts archived by the NOAA Office of Coast Survey (OCS) Historical Map and Chart Collection (`http://chartmaker.ncd.noaa.gov/csdl/ctp/abstract.htm`) were compared with recently published charts. In areas where a difference was evident, soundings and shorelines were manually digitized from the historical chart. The primary source for soundings was the 1966 printing of chart #4132 (Diamond Head to Pearl Harbor Entrance). The 1950 printing of #4132 and 1959 printing of the smaller-scale #4110 (Oahu) were used for comparison, and to ensure that the digitized soundings and shoreline matched the 1960 land condition.

In areas where no substantial difference between the modern and historical charts was observed, the modern survey data used in generation of the primary modeling DEMs were employed.

2.3 Model Setup

By sub-sampling from the DEM described in Section 2.2, three levels of telescoping grids, A, B, and C with increasing resolution of $36''$ (1200 m), $6'$ (200 m) and $1/3''$ (10 m) were used to model tsunami propagation from the deep water offshore of the Hawaiian Islands to the studied coastline (Figs. 5a, b, and c). The A-grid encompasses the major Hawaii Islands and the B-grid covers the Island of Oahu, Penguin Bank, and West Molokai. Run-up and inundation simulations were calculated in C-grid over the study area. A $1/3''$ (10 m) C-grid is necessary to fully resolve the geometry and narrow channels of Pearl Harbor and Honolulu Harbor. In addition, another C-grid with the same $1/3''$ (10 m) resolution based on the 1960 DEM was derived for the simulation of historical destructive tsunamis (Fig. 5d).

For further investigation, 16 virtual gages were systematically distributed in the study area (Fig. 6). Gage 1 was located at the 2-m depth contour at the open coast. Gage 2 represents the Ford Island site. Gages 3 to 16 record the waves propagating into Pearl Harbor. Gage 12 is under the Ford Island Bridge, close to the floating section.

Table 3 summarizes the grid details at each level, and the input parameters for the MOST model. A friction coefficient of 0.00625, which was used for previous Hawaii Standby Inundation Model (SIM) development (Tang *et al.*, 2006), is employed here. Due to the high-resolution grids and large study area, it took about 64 hours of CPU time on a Linux Enterprise system using a single 3.6 GHz Xeon processor for a 4-hour event simulation.

3. Model Validation and Historical Assessment

3.1 Recent Events

Four recent tsunamis from different subduction zones were employed in the model validation. These are the 3 May 2006 Tonga (NZKT $M_w = 8.1$), the 17 November 2003 Rat Islands (AASZ $M_w = 8.1$), the 25 September 2003 Hokkaido (KKJT $M_w = 8.0$) and 23 June 2001 Peru (SASZ $M_w = 8.2$) tsunamis. The Honolulu tide station recorded these tsunami waves with a good signal-to-noise ratio. Figure 7 shows the comparisons of model results and observations at the Honolulu tide station.

The 8.1 M_w 3 May 2006 Tonga earthquake generated a tsunami that was detected about 6 hours later by two offshore tsunameters located to the south of the Hawaiian Islands. These data were combined with the model propagation database to produce the earthquake source by inversion (forthcoming publication). Very good model-observation agreement is obtained at the Honolulu tide gage, including the amplitudes, arrival time, and wave period (Fig. 7a). It correctly models the seventh wave as the largest one over 2 hours later.

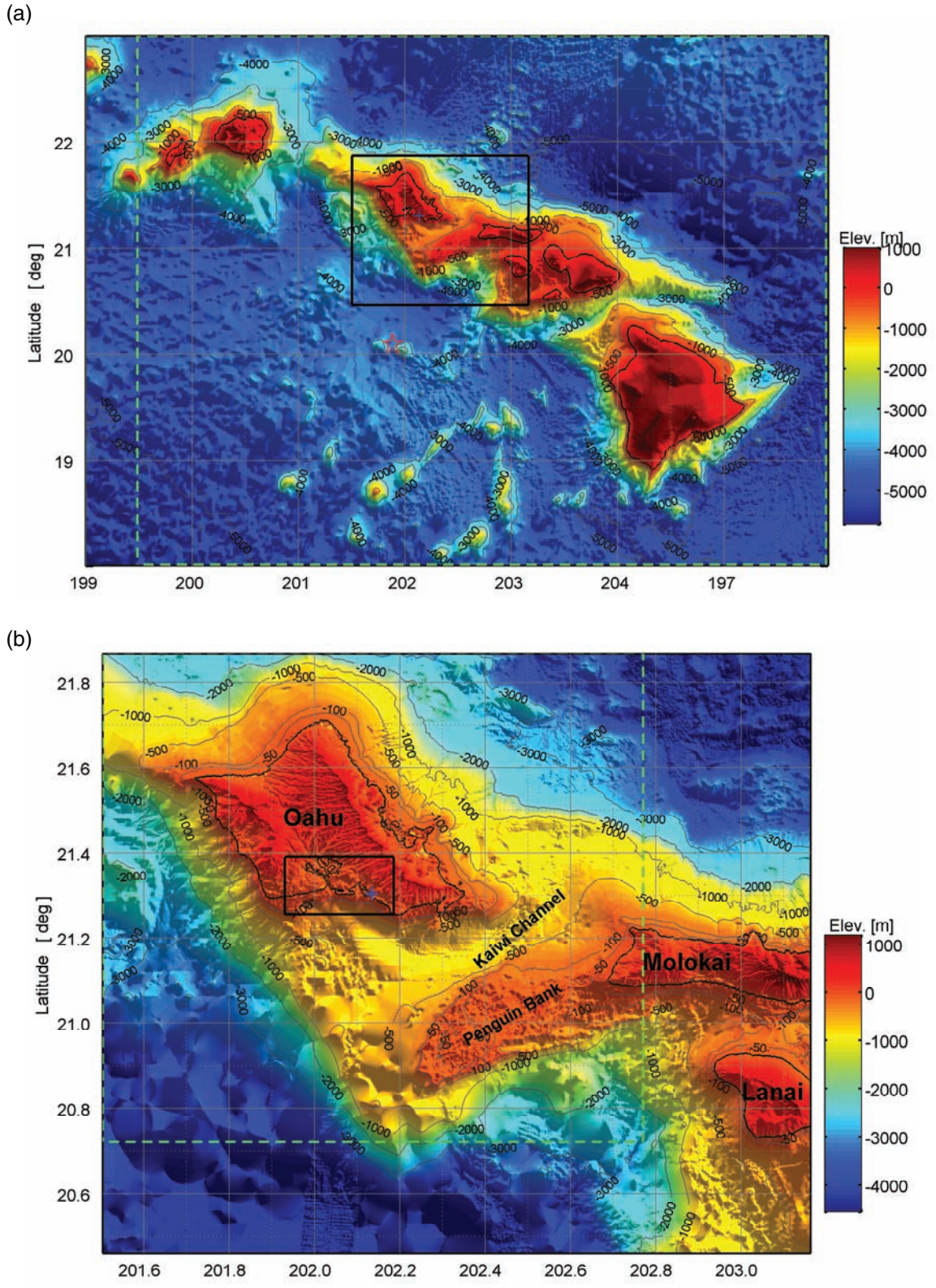

Figure 5: Model computational domains. (a, b, and c) High resolution grids based on 2006 DEM. (d) A C-grid based on 1960 DEM.

(c)

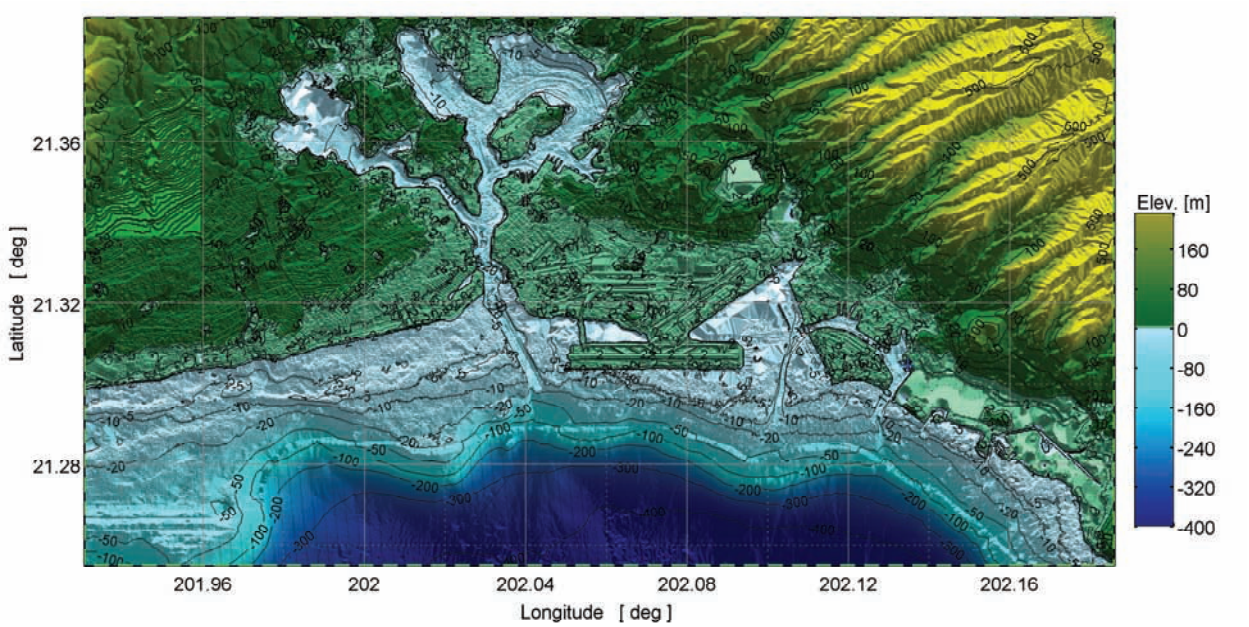

(d)

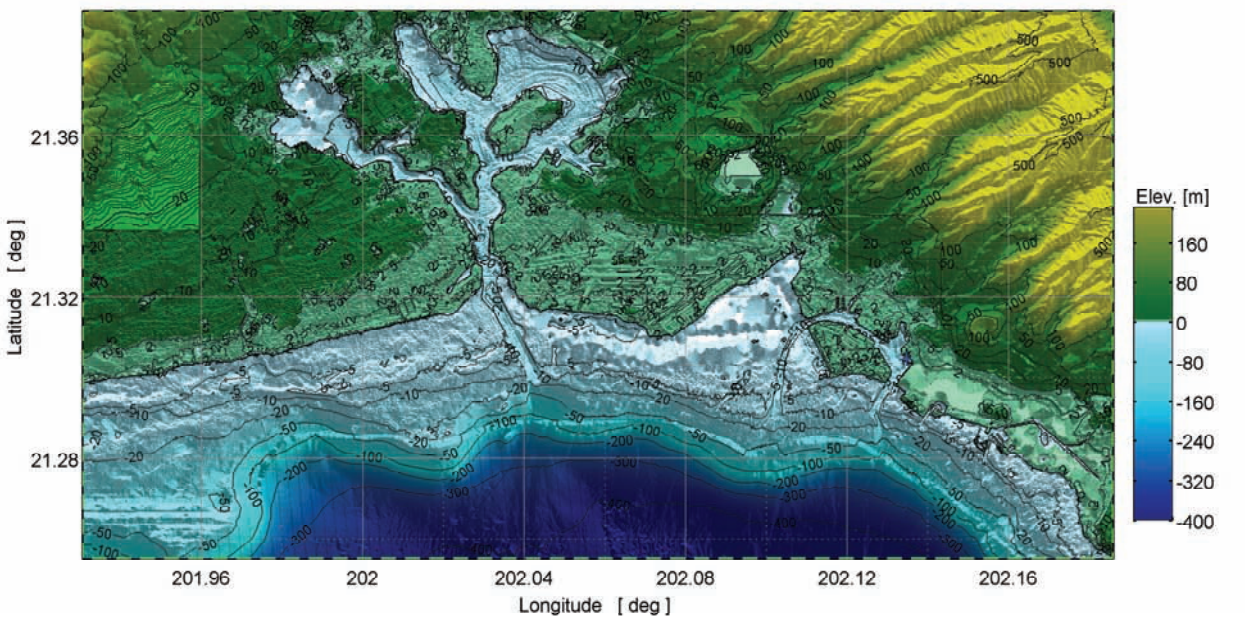

Figure 5: (continued).

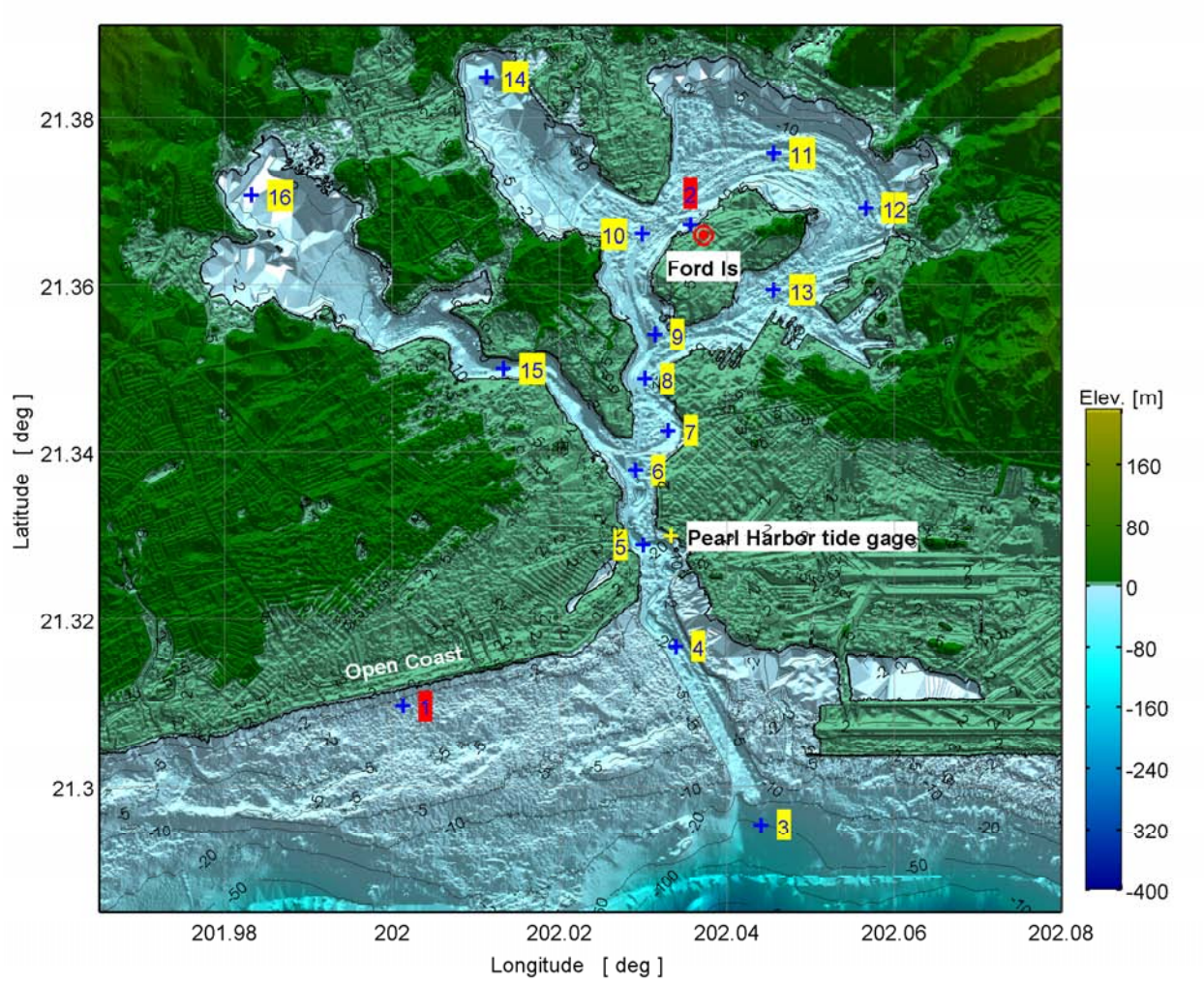

Figure 6: Locations of 16 virtual gages.

Table 3: MOST model setup.

		High Resolution Model		
Grid	**Region**	**Coverage (size) Lon. [°E], Lat. [°N]**	**Cell Resolution [″]**	**Time step [sec]**
A	Hawaii Islands	199–205.98, 18–23 (699×500)	36	1.2
B	Oahu, Penguin bank, & West Molokai	201.5033–203.1633, 20.46–21.8667 (997×845)	6	0.24
C	Pearl Harbor & Honolulu Harbor	201.9306–202.186, 21.255–21.391 (2759×1470)	1/3	0.12
Minimum offshore depth [m]			20	
Water depth for dry land [m]			0.1	
Friction coefficient			0.00625	
CPU time for a 4-hour event simulation			∼64 hours	

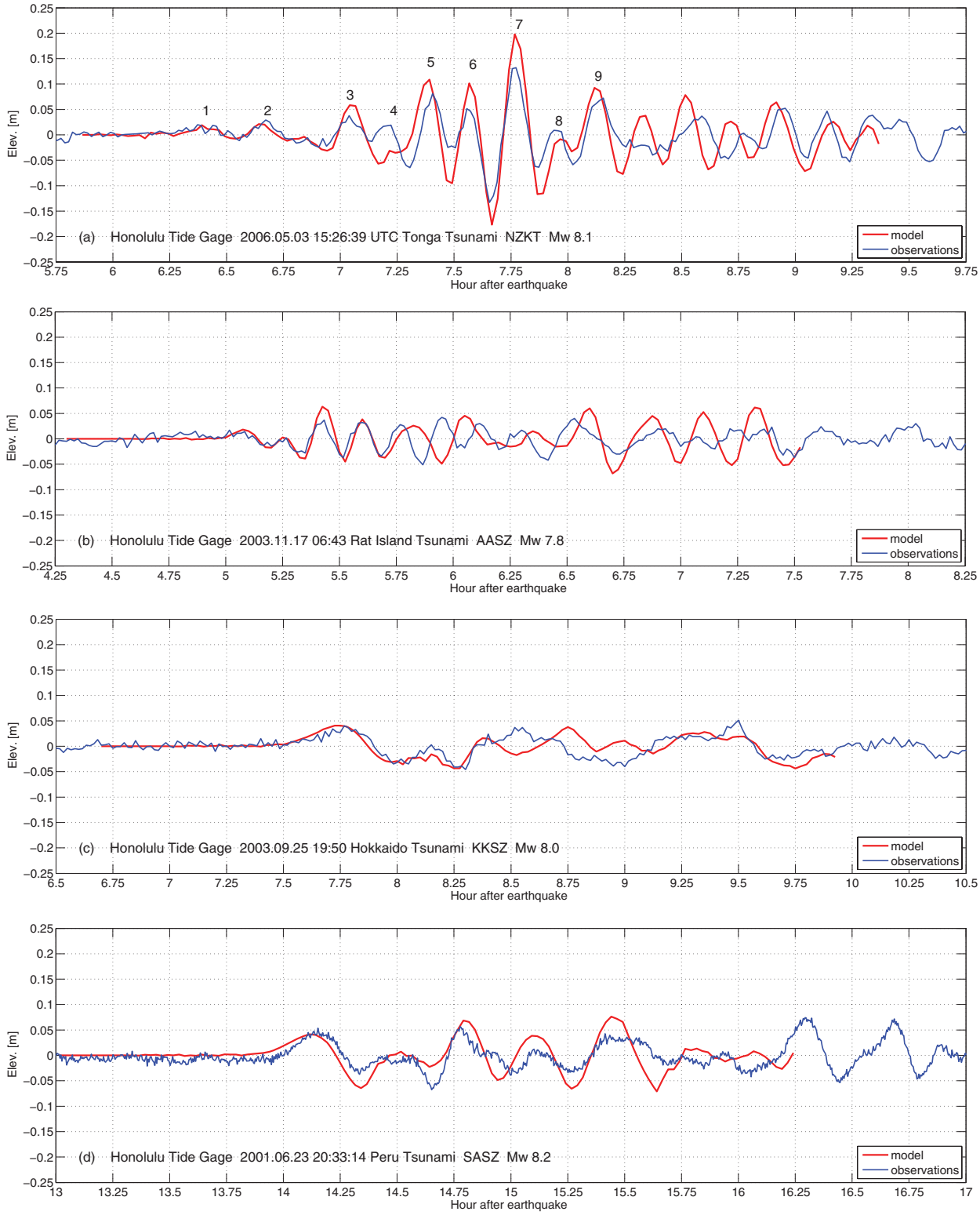

Figure 7: Computed and observed waveforms at Honolulu tide gage for four recent tsunamis.

The 17 November 2003 Rat Islands tsunami was detected by three tsunameters along the Aleutian Trench (Titov *et al.*, 2005). The model predictions also agree quite well with the Honolulu tide gage observations (Fig. 7b).

The shallow 25 September 2003 Hokkaido earthquake generated tsunami waves with an extraordinarily long period. The Honolulu tide station recorded its first wave with a period of more than 48 min. Figure 7c demonstrates that amplitudes, arrival time, and period of the first several waves of the wave train were correctly modeled.

No tsunameter data is available for the 23 June 2001 Peru tsunami. The earthquake source characteristics were derived from an inversion of the coastal Kahului tide gage data using the Kahului SIM (Tang *et al.*, 2006). The 8.2 earthquake magnitude estimated by this process is consistent with seismic data from the Revised Harvard CMT model. It gives good model-observation comparison at the Honolulu tide gage (Fig. 7d).

3.2 The Five Destructive Tsunamis

The limited number of tsunameter (DART) records does not include any of the destructive tsunamis described in section 2.1. Previous studies of seismic, geodetic, and water-level data have established the possible source parameter for some of the events (Kanamori and Ciper, 1974; Johnson *et al.*, 1994, 1996; Johnson and Satake, 1999). However, those sources are subject to debate and adjustment. Most of the source estimates that have been done are based on low-resolution tsunami propagation models. The Standby Inundation Models (SIMs) that have been developed at NCTR provide a unique chance to re-investigate the historical sources by inversion of the water level data with the high-resolution quality inundation and propagation models. Preliminary results are available for the 1964, 1957, 1952, and 1946 tsunamis.

The 28 March 1964 Alaska tsunami is the best documented of the historical events. Water-level data (Spaeth and Berkman, 1967) are available for ten of the SIM sites developed to date. The slip distribution of the source was then determined by inversion of data from two coastal tide stations, Kahului in Hawaii and Yakutat in Alaska. The details will be published in a forthcoming NCTR report. In total, 50 unit sources covering the aftershock area were employed in the study. Figure 8a shows the source locations and the slip distribution. The tsunami source area with the highest slip is found on the east side of Kodiak Island, giving a magnitude of 9.0 M_w. It produces excellent model comparison with observations at the Honolulu tide gage (Fig. 8b).

The 9 March 1957 Andreanof Islands tsunami was one of the tsunamis with the longest aftershock zones ever recorded, at 1200 km (Johnson *et al.*, 1994). Unit sources 1 to 12 of the A and B lines along the AASZ subduction zone were selected to characterize the source. The inversion using the Kahului and Crescent City SIMs gives a magnitude of 8.7 M_w and the slip distribution shown in Fig. 9a. The small slip in the eastern part of the rupture zone (A10) generated a very small first wave at Kahului and the first two or three waves at Crescent City. The large slip near the western

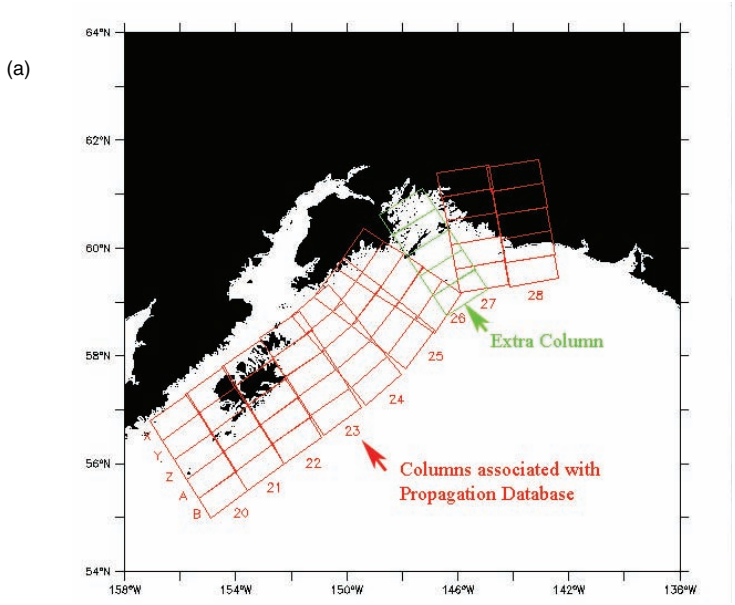

	20	21	22	23	24	25	26	267	27	28
X	0	0	0	5	3	10	0	0	0	0
Y	0	0	0	37	14	0	0	0	0	0
Z	0	0	5	38	29	0	0	0	0	0
A	0	0	4	28	2	0	0	0	0	0
B	0	0	0	0	0	0	0	0	0	0

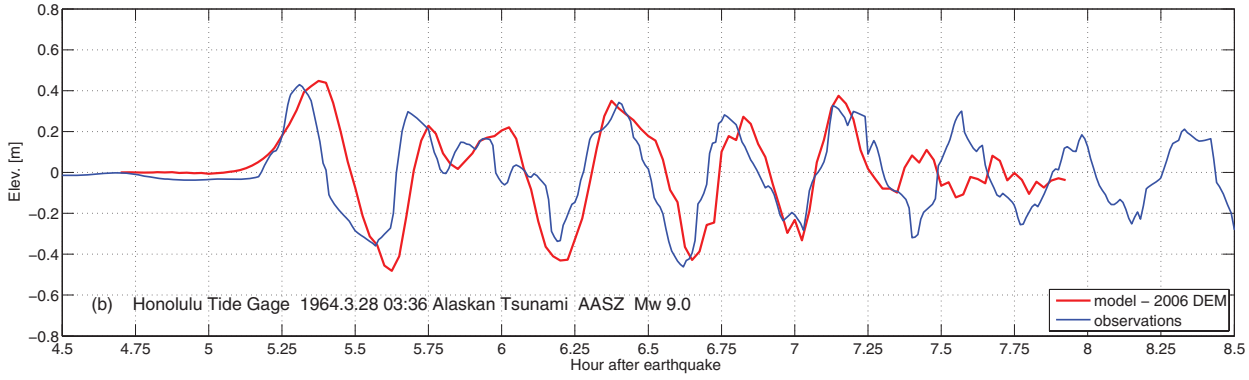

Figure 8: The 1964 Alaskan tsunami ($M_w = 9.0$). (a) Location and slip distribution (m) of unit sources. (b) Computed and observed waveforms at Honolulu gage.

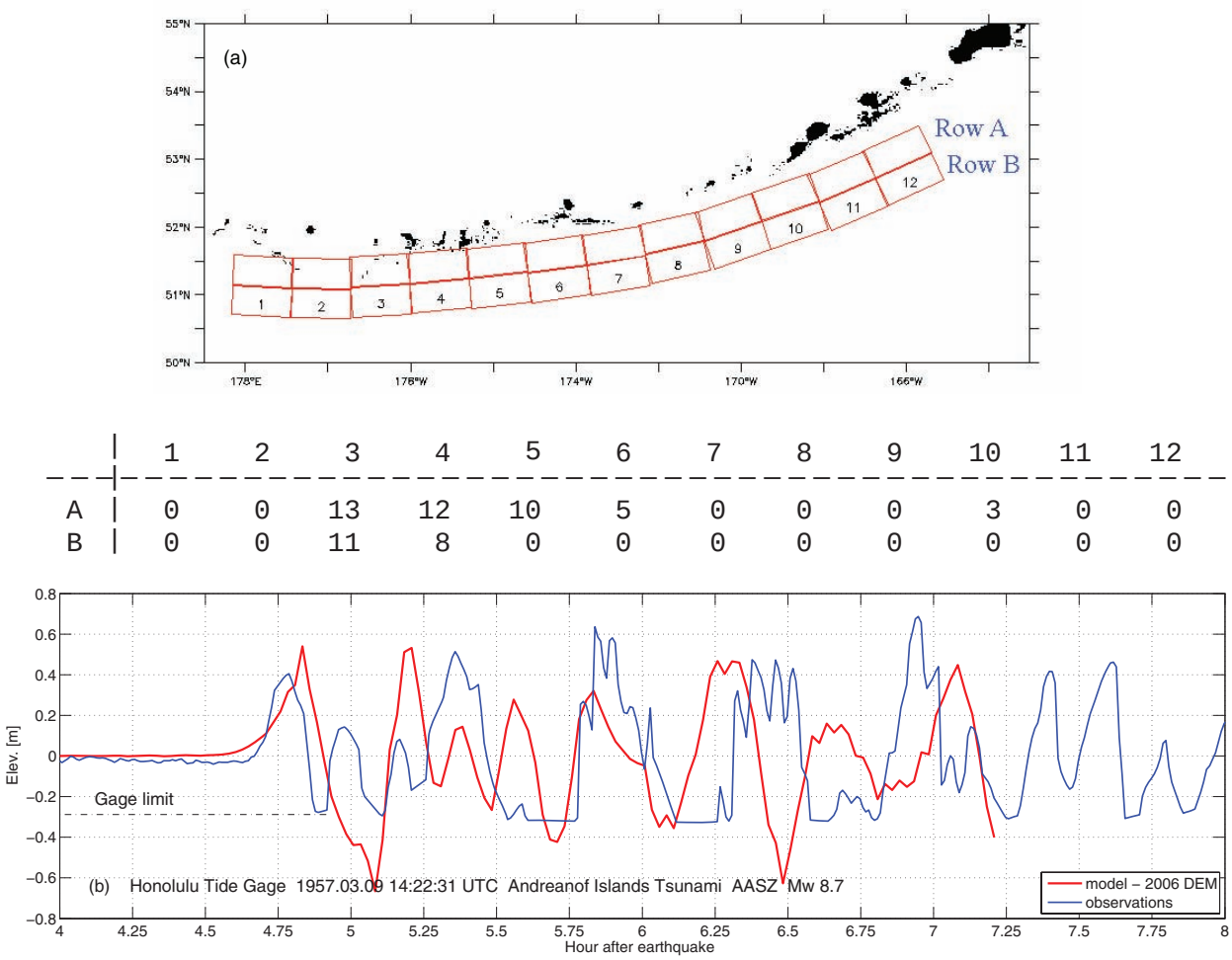

Figure 9: The 1957 Andreanof tsunami (M_w = 8.7). (a) Location and slip distribution (m) of the unit sources. (b) Computed and observed waveforms at Honolulu gage.

end of the rupture zone caused the large major waves in Kahului and large later waves at Crescent City. Figure 9b shows a reasonable comparison of computed and observed waveforms at the Honolulu tide gage.

Certain difficulties arise in the determination of the 4 November 1952 Kamchatka tsunami source. First, none of the SIMs available to date lies close to the earthquake source. Second, the Hawaiian SIMs with water level data are located at either the south or east shore of the islands, while the incoming waves were from the northwest. In addition, located perpendicular to the Kamchatka subduction zone, Hawaiian SIMs are in the least favorable arrangement for inversion, since the travel times from the unit sources of the Kamchatka subduction zone to Hawaii do not vary significantly. Inversion using the Hilo tide gage data gives a first estimate of the slip distribution. The wave amplitude was underestimated at the Honolulu gage, but overestimated at the Pearl Harbor gage (Fig. 10).

In Hawaii, only the Honolulu tide station was available to record data for the 1 April 1946 tsunami. Inversion of the data gives a magnitude of 8.5.

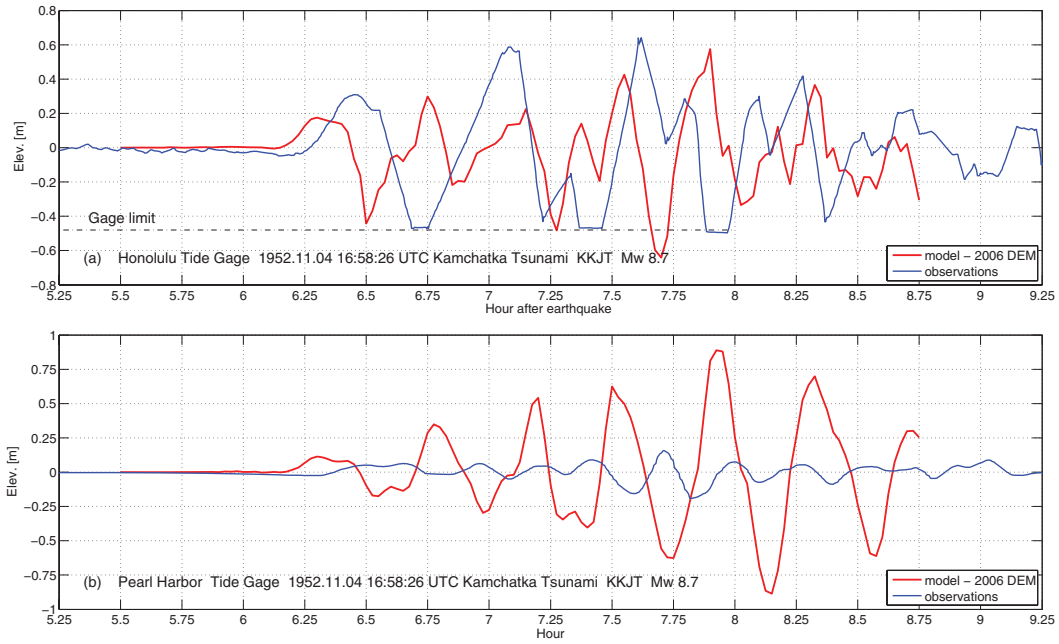

Figure 10: Comparison of computed and observed waveforms at (a) Honolulu gage and (b) Pearl Harbor gage for the 1952 Kamchatka tsunami.

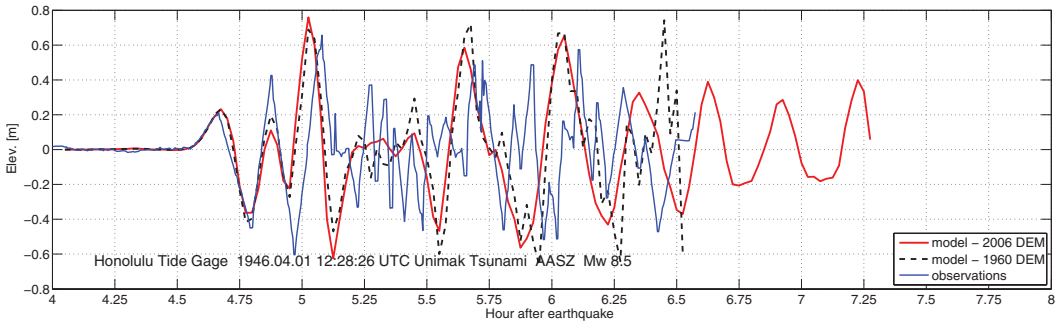

Figure 11: Comparison of observed and computed waveforms using 2006 and 1960 DEMs at Honolulu gage for the 1946 Unimak tsunami.

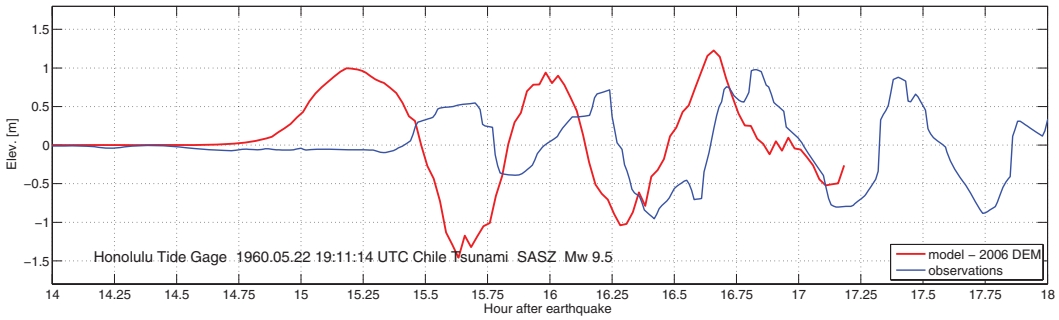

Figure 12: Comparison of computed and observed waveforms at Honolulu gage for the 1960 Chile tsunami.

A good comparison of model and observations was obtained (Fig. 11). The third wave is the largest. Figure 11 also shows the computed waveform using the 1960 DEM, which gives essentially the same result as the 2006 DEM.

The fault parameters of the 22 May 1960 Chile tsunami are taken from Kanamori and Ciper (1974). These give a reasonable comparison of the wave amplitude and period to the Honolulu tide gage data (Fig. 12). The computed arrival time is about 20 min earlier than the observations.

There is no credible inundation data inside Pearl Harbor. Comparison of model results with other nearby areas covered in more detail by Walker (2004) is a potential subject for further study.

3.3 Impacts to Study Area

Figures 13, 14, and 15 show the computed maximum wave amplitudes and velocities for the nine historical tsunamis. In general, the open coast outside Pearl Harbor experienced large waves. The 1946 tsunami was used to study the effect of the changed Honolulu coastline. From Figs. 15a and 15b we can see that the coral reef runway has only local effects. The waveforms at gages 1 to 16 indicate the change is negligible (Fig. 15c).

Starting from Gage 3 in 50-m isobath, the wave propagates toward the Pearl Harbor entrance (G4), with increasing amplitude due to shoaling. In the Main Channel, from G4 to G6, the amplitude is similar because of the constant water depth. Then the Entrance Channel divides into the West Loch (G15 to 16) and the East Branch (G7 to G9), with the East Branch further divided into Middle Loch (G9-10-14) and East Loch (G9-13-12-11) by Ford Island. While the wave in the West Loch has the same amplitudes as the Main Channel, the amplitude decreases significantly in the Middle and East Lochs (Fig. 14c).

Figure 16 compares the waveforms at Gages 1 and 2 for the nine historical tsunamis. With typical incident wave periods of 24 min or less at Gage 1, the maximum wave amplitude at the open coast is significantly larger than at Ford Island (5 to 8 times). With a longer period such as the approximately 32-min waves for the 2001 Peru and 1964 Alaska tsunamis, resonance starts to appear inside Pearl Harbor (Figs. 16.4 and 16.5). With the extraordinarily long periods of the 2003 Hokkaido (48 min) and 1960 Chile (60 min) tsunamis, Gage 2 clearly shows the influence of the characteristic resonance with a period around 96 min for Pearl Harbor. For these two events, the maximum wave amplitude at Ford Island is close or equal to that of the open coast. More details of the resonance are shown in Fig. 17, which shows the computed waveforms at gages 3 to 16 for the 2003 Hokkaido tsunami.

There was no significant inundation at Ford Island during these historical events. Land elevation is 3.4 m for the candidate site on Ford Island, while it is about 1.6 m above MHW for the open coast. The shore LIDAR data show a long narrow dune along the open coast with an elevation of about 2 m. This dune has protected the open coast from destructive tsunamis.

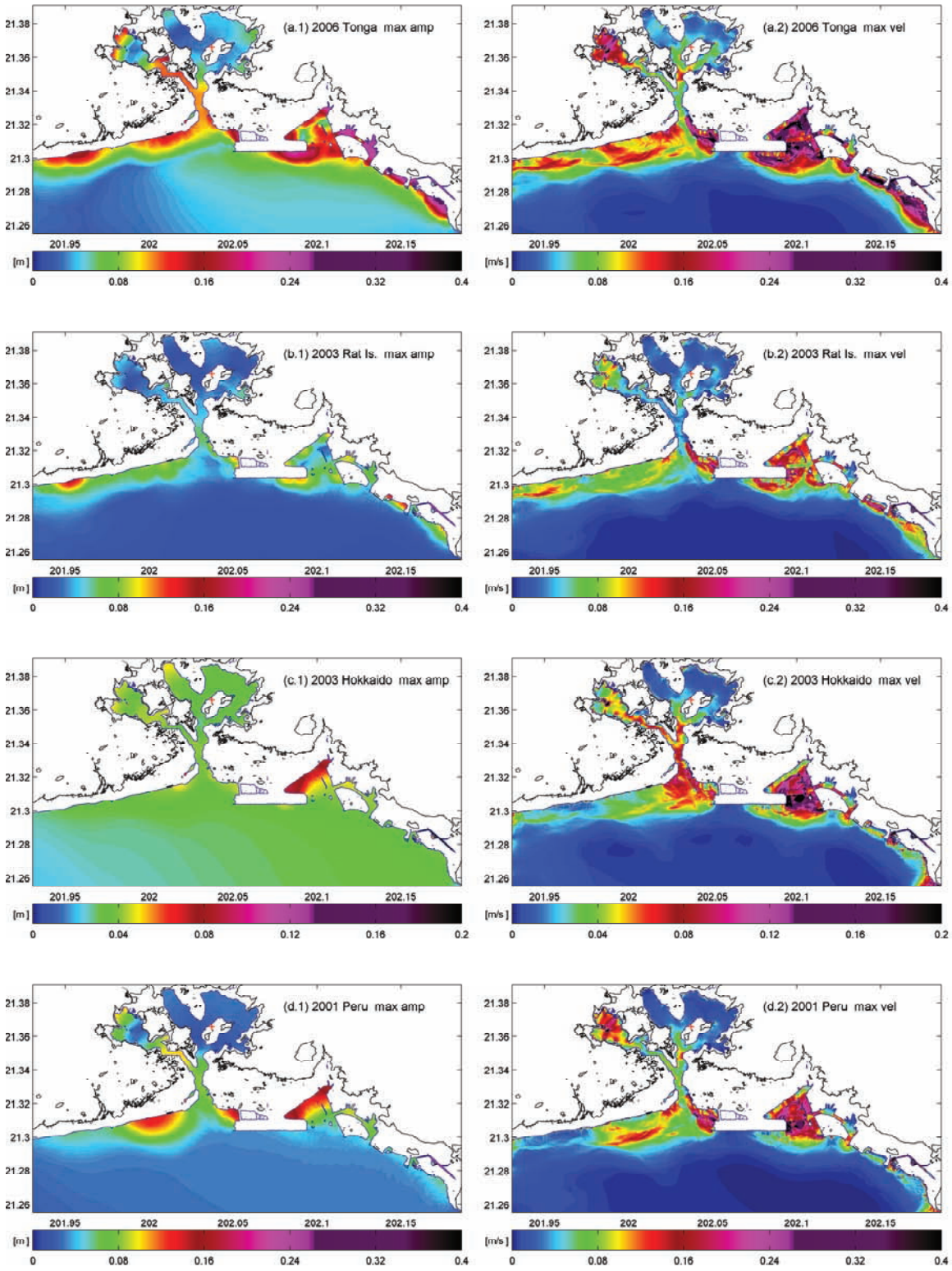

Figure 13: Computed maximum wave amplitude and velocity for the four recent tsunamis. (Reference: 2 m/s = 1 knot).

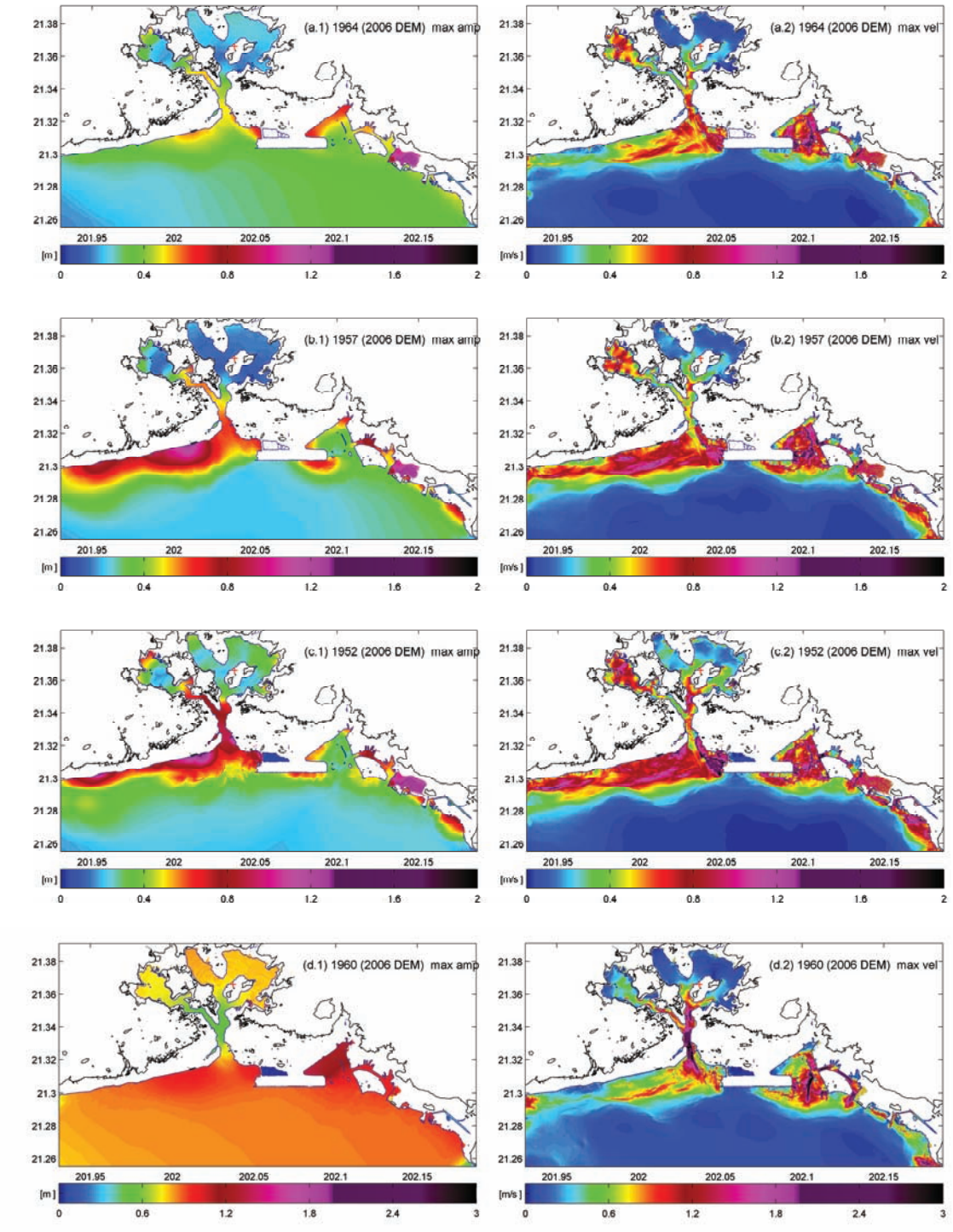

Figure 14: Computed maximum wave amplitude and velocity for the (a)1964, (b) 1957, (c) 1952 and (d) 1960 tsunamis.

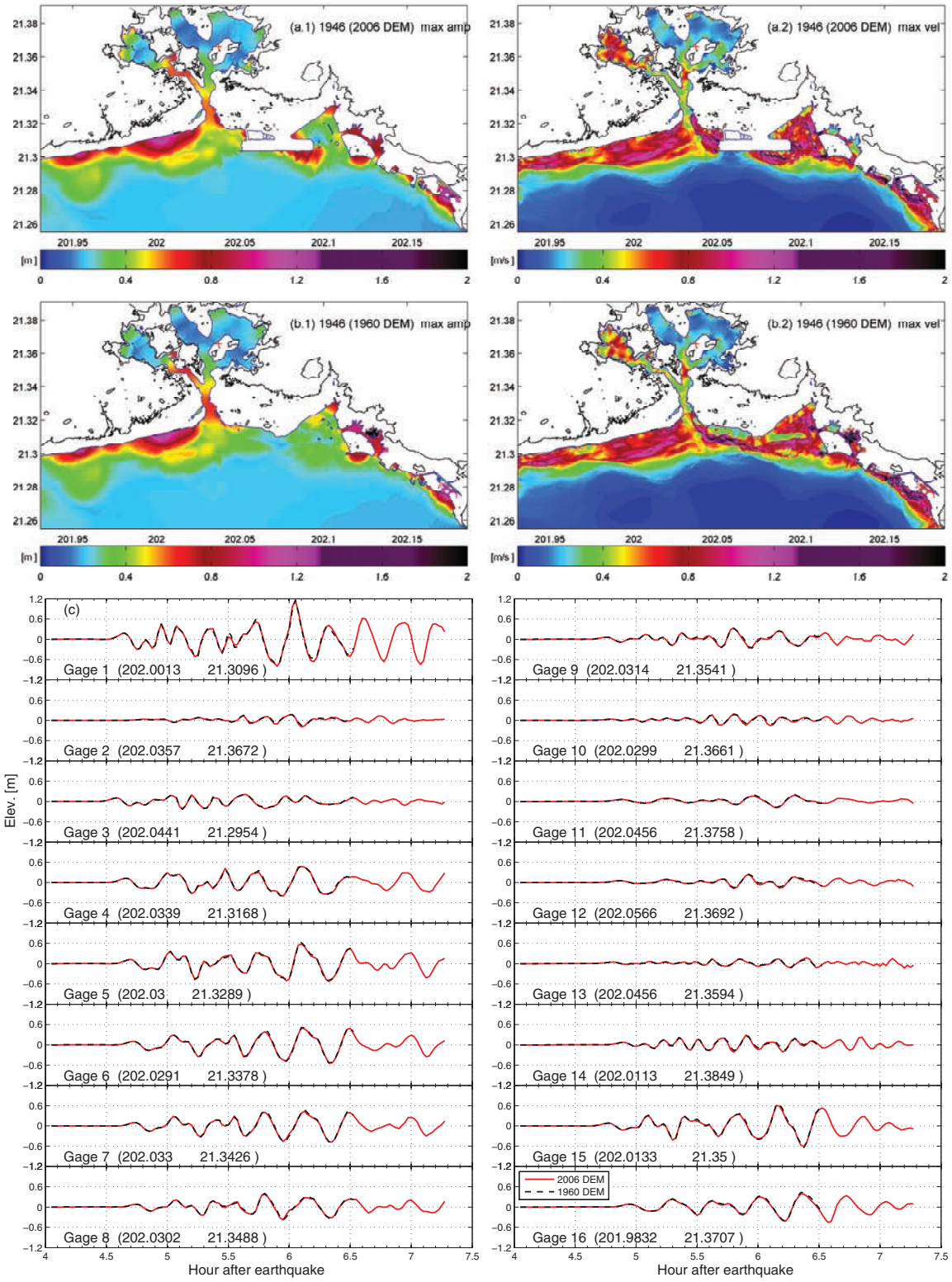

Figure 15: Comparison of model results from 2006 and 1960 DEMs for the 1946 tsunami. (a and b) Maximum wave amplitude and velocity. (c) Waveforms at gages 1–16.

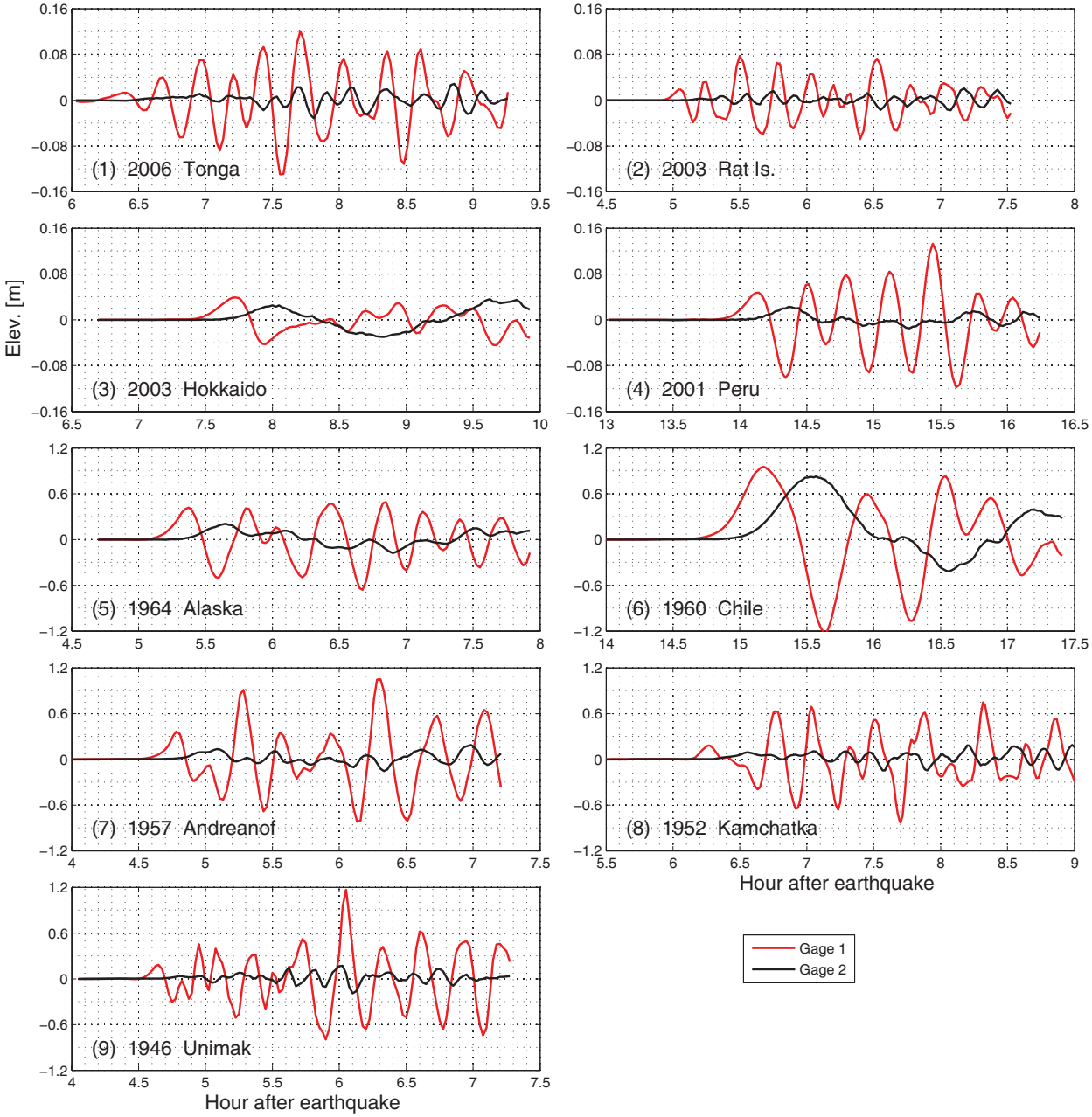

Figure 16: Comparison of computed waveforms at the open coast (Gage 1) and Ford Island (Gage 2) for the nine historical tsunamis.

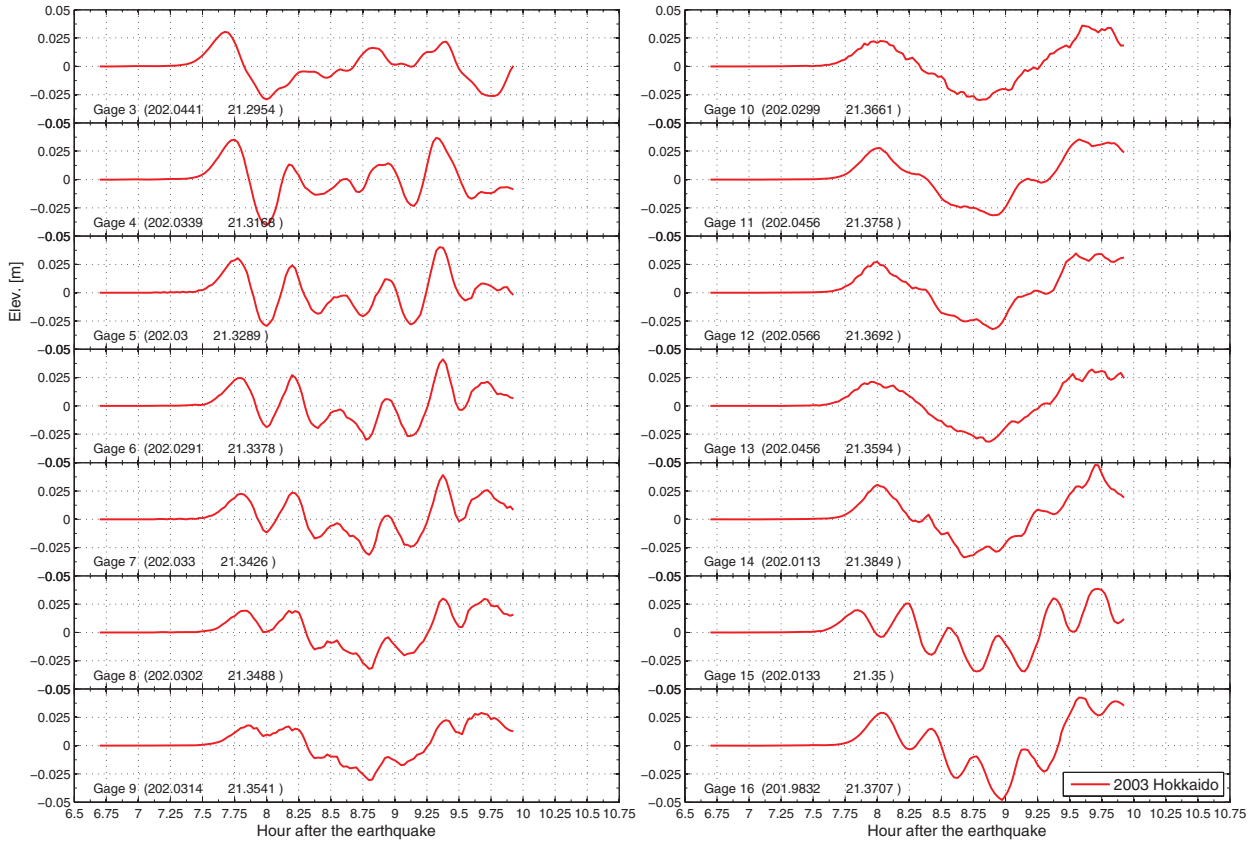

Figure 17: Computed waveforms at gages 3–16 for the 2003 Hokkaido tsunami.

4. Worst-Case Scenario Assessment

Recorded historical tsunamis provide only a limited number of events, from limited locations. More comprehensive test cases are needed in order to identify the most dangerous scenarios that may cause devastating impacts in the study area.

To address this problem, a set of 18 simulated tsunamis with 9.3 M_w was carefully selected as follows. Based on the pre-computed propagation database, the first arrival and maximum wave amplitude at a site offshore of Pearl Harbor were computed. The results are shown in Fig. 18. Then, from each subduction zone, a 9.3 M_w tsunami was simulated for the section that generates the maximum of maximum offshore wave amplitudes. More attention was required for the Kamchatka source to the northwest and the Aleutian Islands to the north. The propagation model database, with its lower spatial resolution, is likely to inadequately represent waves arriving in the lee of significant bathymetric features. Therefore, more than one simulated tsunamis from KKJT and AASZ were included in the study. Figure 18 also shows the sources of the 18 simulated tsunamis, starting from the Japan Trench and continuing clockwise around the Pacific Ocean.

Each simulated earthquake involves 20 unit sources (10 pairs) and a uni-

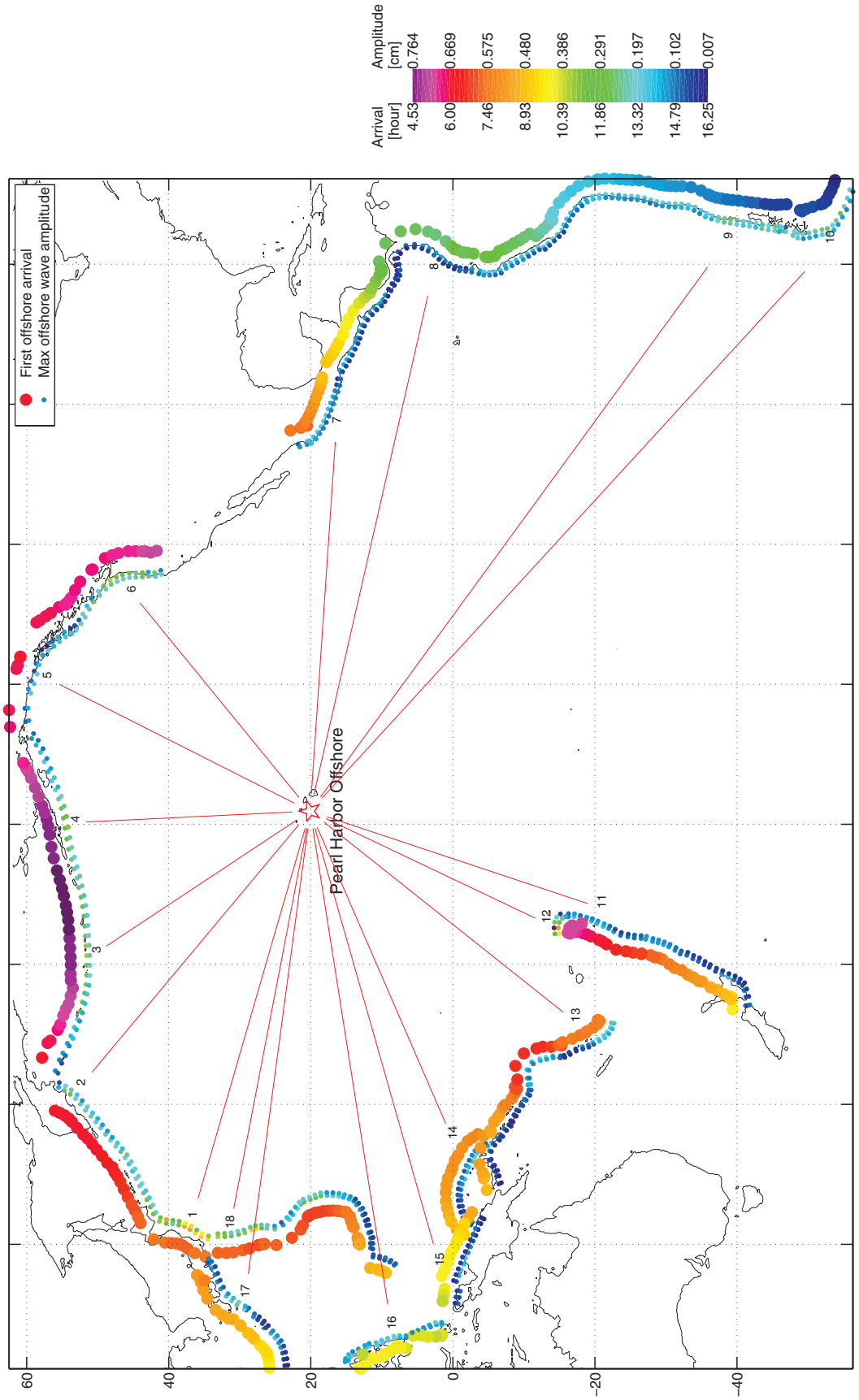

Figure 18: First arrival and maximum wave amplitude at Pearl Harbor offshore. Dot points also indicate unit source centers. Red lines show simulated tsunamis involved in this study.

form 29-m slip. The 10 pairs of unit sources along the Cascadia Subduction Zone involve the whole subduction zone. Since it takes about 64 hours of CPU time for a simulation with the 1/3″ (10 m) high-resolution model, a set of test grids with 1″ (30 m) resolution were developed for use in the search for the worst-case scenario. The details of the test model and other results are presented in Appendix A.

Figure 19 shows the test model results of computed waveforms at Gages 1 and 2 for the 18 simulated tsunamis. It is clear that the open coast experiences more severe impacts than Ford Island. Eight of them generate inundation at the open coast, while no significant inundation is generated at Ford Island (Fig. A1). Tsunamis that could potentially cause severe impacts to the study area can be generated from the Kamchatka, East Philippine, Japan, Alaska-Aleutian, South American, and Cascadia Subduction Zones. The unit source NZKT B38 to the north of Tonga has the maximum offshore amplitude among the entire unit sources.

Since a tsunami from Kamchatka (No. 2) causes the most severe inundation, it was selected as the worst-case scenario. The simulation was then rerun using the high-resolution model; the results are shown in Fig. 20. The maximum wave amplitude reaches 3.75 m at the open coast, while it is 0.6 m for Ford Island.

5. Concluding Remarks

Focusing on the distant-source tsunamis, this study provides numerical modeling results of a 1/3″ (10 m) high-resolution inundation model for assessment of potential tsunami impact for Pearl Harbor, Hawaii. It was based on available information on past distant-source tsunamis striking Pearl Harbor, as well as on scenarios of distant tsunamis from the major subduction zones throughout the Pacific Region. The tsunami model used the best available data on water depths and land elevations, including any recent changes in either.

Nine historical tsunamis were used in the study: four recent events with high-quality DART and tide-gage data and five destructive tsunamis in Hawaiian history. Excellent model-observation agreement was obtained for the four recent events as well as the 1964 Alaska and 1946 Unimak tsunamis. The model yielded reasonable comparisons for the 1952 Kamchatka, 1957 Andreanof, and 1960 Chile tsunamis. In addition, the study examined 18 simulated 9.3 M_w tsunamis from all major subduction zones using a test inundation model with 1″ (30 m) resolution. The comprehensive modeling results indicate that hazardous wave conditions are likely to be created in the study area by tsunamis originating from the Kamchatka, East Philippine, Japan, Alaska-Aleutian, South American, and Cascadia Subduction Zones. In particular, the Kamchatka scenario produces the most severe impact on the study site. The unit source NZKT B38, to the north of Tonga, has the maximum offshore amplitude from a single unit source.

Larger wave heights and higher velocities are found in the Entrance Channel, the West Loch, and the channel near Hospital Point. With a typical

Figure 19: Comparisons of computed wave amplitude at the open coast (Gage 1) and Ford Island (Gage 2) for 18 simulated M_w 9.3 tsunamis. Results are from the 1″ test model.

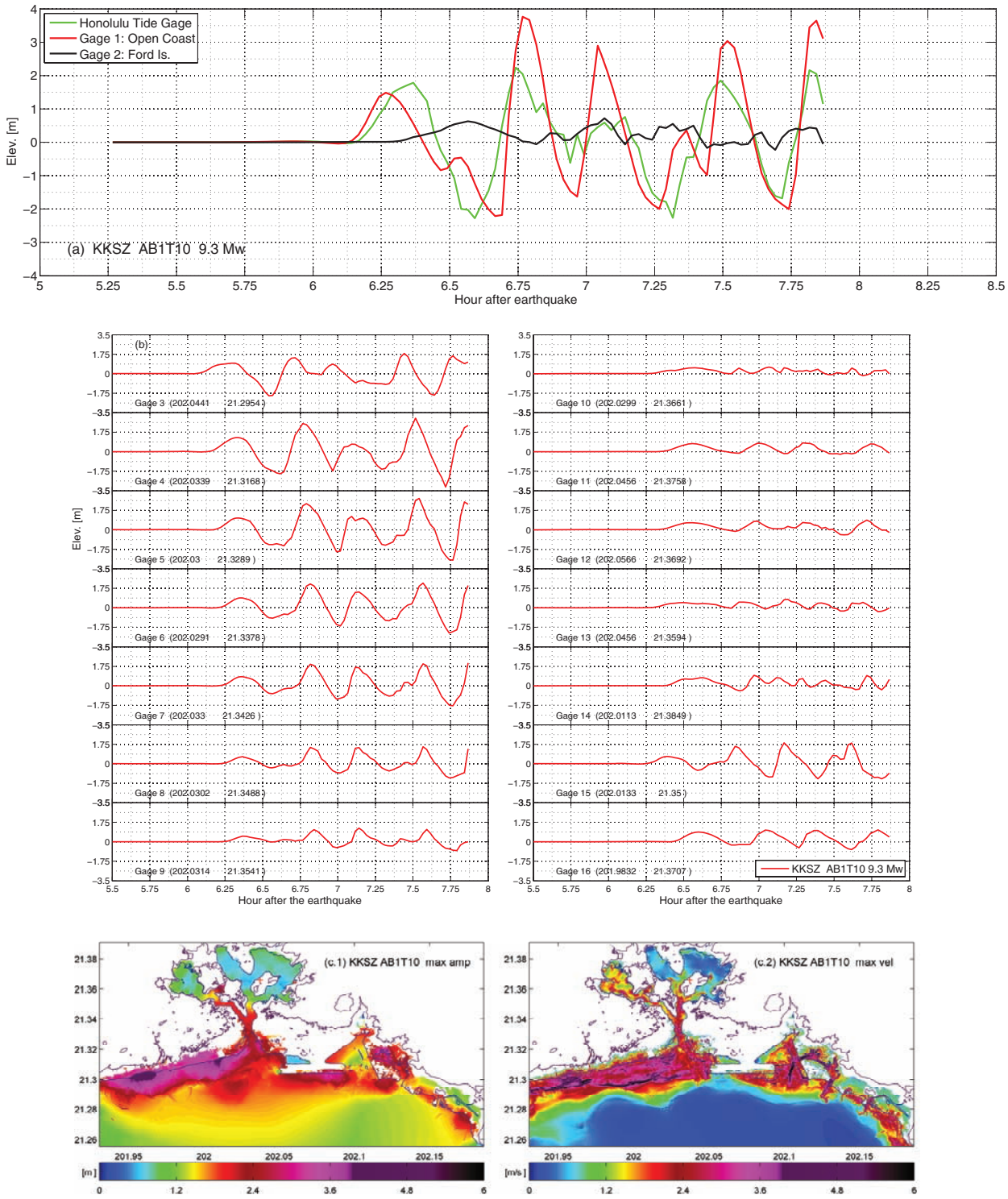

Figure 20: The worst-case scenario: a simulated M_w 9.3 tsunami from Kamchatka. Computed waveforms at (a) Honolulu gage, the open coast (Gage 1) and Ford Island (Gage 2), (b) at Gages 3 to 16. (c) Maximum wave amplitude and velocity. Results are from the $1/3''$ high-resolution model.

incident wave period of 24 min or less, the north shore of Ford Island experiences significantly smaller waves than the open coast. When the typical incident wave period reaches 48 min or more, a characteristic resonance with a period around 96 min at Pearl Harbor is excited, resulting in similar maximum wave amplitudes both inside Pearl Harbor and on the open coast.

The results of the study show that none of the tsunamis observed in the past nor any of the 18 modeled scenario events—based on great subduction zone earthquakes—have caused inundation at the NOAA building site.

Modeling results indicate that changes in the Honolulu coastline since 1940 have little effect on the waveforms in both Pearl Harbor and Honolulu Harbor.

6. Acknowledgments

This study was funded by NOAA. Special thanks to Drs. David Burwell, Edison Gica, Robert Weiss, Diego Arcas, and Yong Wei in the NCTR Modelers' group for assistance with the historical tsunami sources; thanks as well to Marie Eble for assistance with DART and tide gage data and to Jean Newman for help with the propagation database.

This publication is partially funded by the Joint Institute for the Study of the Atmosphere and Ocean (JISAO) under NOAA Cooperative Agreement No. NA17RJ1232, Contribution #1339.

7. References

Berkman, S.C., and J.M. Symons (1964): The tsunami of May 22, 1960 as recorded at tide stations. Coast and Geodetic Survey, 79 pp.

Gica, E., M. Spillane, V.V. Titov, and C. Chamberlin (2006): Development of the forecast propagation database for the NOAA Tsunami Forecasting System. NOAA Tech. Memo, OAR PMEL (in review).

Green, C.K. (1946): Seismic sea wave of April 1, 1946, as recorded on tide gages. *Trans. AGU, 27*(4), 490–500.

Jonson, J.M., Y. Tanioka, L.J. Ruff, K. Satake, H. Kanamori, and L.R. Sykes (1994): The 1957 Great Aleutian Earthquake. *Pure Appl. Geophys., 142*, 3–28.

Johnson, J.M., K. Satake, S.R. Holdahl, and J. Sauber (1996): The 1964 Prince William earthquake: Joint inversion of tsunami and geodetic data. *J. Geophys. Res., 101*(B1), 523–532.

Johnson, J.M., and K. Satake (1999): Asperity distribution of the 1952 Great Kamchatka earthquake and its relation to future earthquake potential in Kamchatka. *Pure Appl. Geophys., 154*(3–4), 541–553.

Kanamori, H., and J.J. Ciper (1974): Focal process of the great Chilean earthquake, May 22, 1960. *Phys. Earth Planet. Int., 9*, 128–136.

Kimberly, S.M. (1993): An ecological perspective on inshore fisheries in the main Hawaiian Islands. (Fisheries of Hawaii and U.S.-Associated Pacific Islands). *Mar. Fish. Rev.*, 3/22/1993.

Lander, J.F., and P.A. Lockridge (1989): *United States Tsunamis* (Including United States Possessions) 1690–1988. National Oceanic and Atmospheric Administration, National Geophysical Data Center, Boulder, Colorado, USA, Publication 41-2, 265 pp.

National Geophysical Data Center, Global Tsunami Database (2000 BC to present): `http://www.ngdc.noaa.gov/seg/hazard/tsu\_db.shtml`.

Shepard, F.P., G.A. Macdonald, and D.C. Cox (1950): Tsunami of April 1, 1946, *Bull. Scripps Inst. Oceanogr., 5*, 391–528.

Spaeth, M.G., and S.C. Berkman (1967): The Tsunami of March 28, 1964, as Recorded at Tide Stations. Coast and Geodetic Survey Technical Bulletin No. 33, Rockville, MD, July 1967.

Pararas-Carayannis, G., and J.P. Calebaugh (1977): *Catalog of Tsunamis in Hawaii*. World Data Center A for Solid Earth Geophysics, Report SE-4, 78 pp.

Tang, L., C. Chamberlin, V.V. Titov, and E. Tolkova (2006): A standby inundation model of Kahului, Hawaii for NOAA Short-term Inundation Forecasting for Tsunami (SIFT). NOAA Technical Memorandum OAR PMEL (in review).

Titov, V.V., F.I. González, E.N. Bernard, M.C. Eble, H.O. Mofjeld, J.C. Newman, and A.J. Venturato (2005): Real-time tsunami forecasting: Challenges and solutions. *Nat. Hazards, 35*(1), Special Issue, U.S. National Tsunami Hazard Mitigation Program, 41–58.

Titov, V.V., and C.S. Synolakis (1998): Numerical modeling of tidal wave runup. *J. Waterw. Port Coast. Ocean Eng., 124*(4), 157–171.

Titov, V.V., and F.I. González (1997): Implementation and testing of the Method of Splitting Tsunami (MOST) model. NOAA Technical Memorandum ERL PMEL-112, NOAA Pacific Marine Environmental Laboratory, 11 pp.

Walker, D.A. (2004): Regional Tsunami evacuations for the state of Hawaii: A feasibility study on historical runup data. *Sci. Tsunami Haz., 22*(1), 3–22.

Zerbe, W.B. (1953): The tsunami of November 4, 1952 as recorded at tide stations. Coast and Geodetic Survey, Special Publication No. 300, 62 pp.

Appendix A. Test Model Setup and Results

A test inundation model with 1″ resolution was developed for Pearl Harbor to quickly locate the worst-case scenarios among the 18 simulated 9.3 M_w tsunamis described in section 4. Table A1 summarizes the grid details at each level, and the input parameters for the MOST model. The model was also validated by the nine historical tsunamis. The computed maximum wave amplitude and velocity are plotted in Fig. A1. Eight of the 18 simulated tsunamis caused inundation at Ewa Beach while there was no inundation at Ford Island.

Table A1: Setup for the 1″ test model.

		Test Model		
Grid	**Region**	**Coverage (size) Lon. [°E], Lat. [°N]**	**Cell Resolution [″]**	**Time step [sec]**
A	Hawaii Islands	199.4833–205.9633, 18–23 (217×167)	108	4
B	Oahu & Penguin bank	201.5033–202.77, 20.7217–21.8683 (381×345)	12	0.8
C	Pearl Harbor & Honolulu Harbor	201.9306–202.1895, 21.255–21.391 (920×490)	1	0.4
Minimum offshore depth [m]			20	
Water depth for dry land [m]			0.1	
Friction coefficient			0.00625	
CPU time for a 4-hour event simulation			∼3 hours	

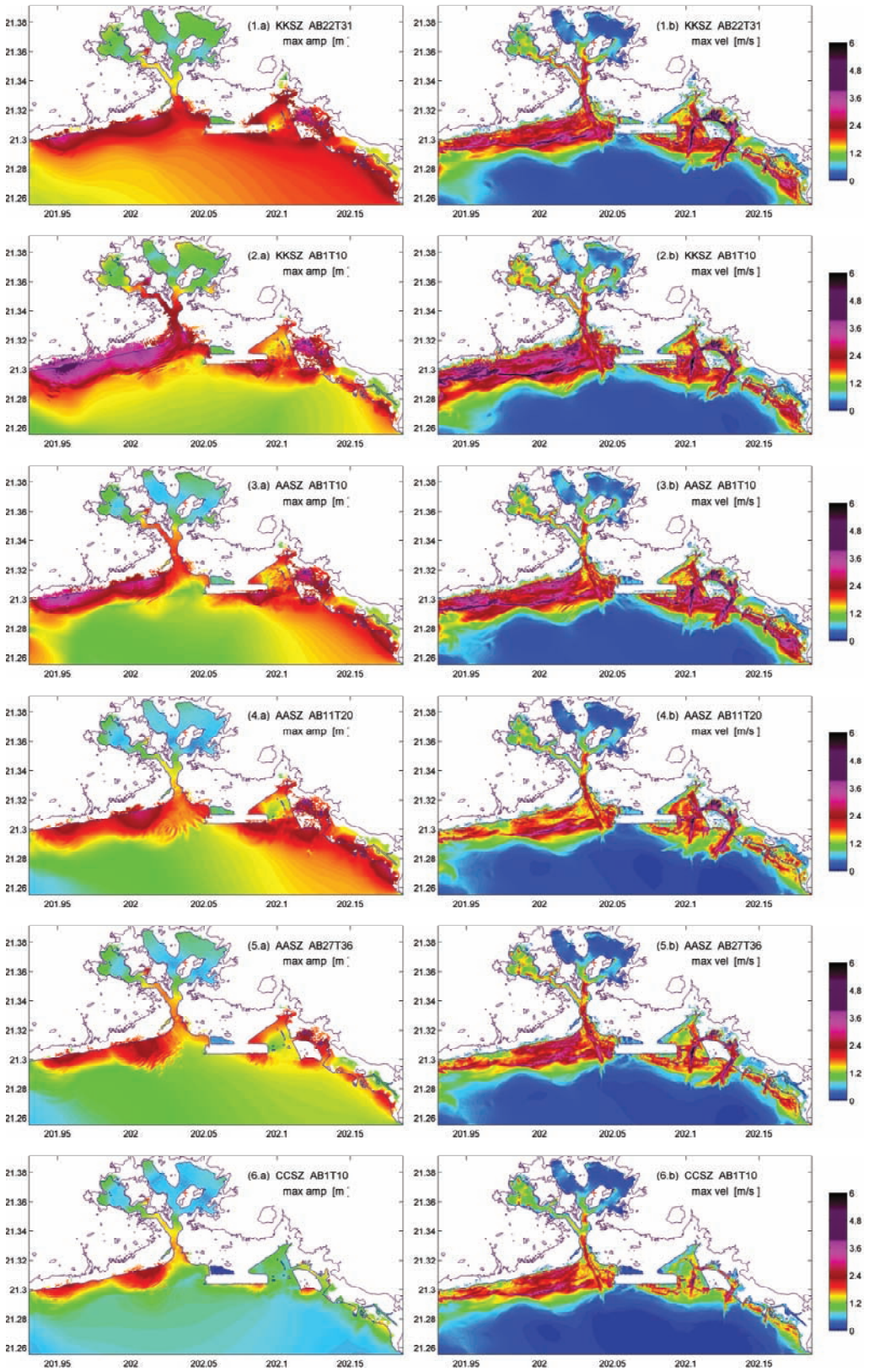

Figure A1: (a) Maximum wave amplitude and (b) velocity for 18 simulated 9.3 M_w tsunamis.

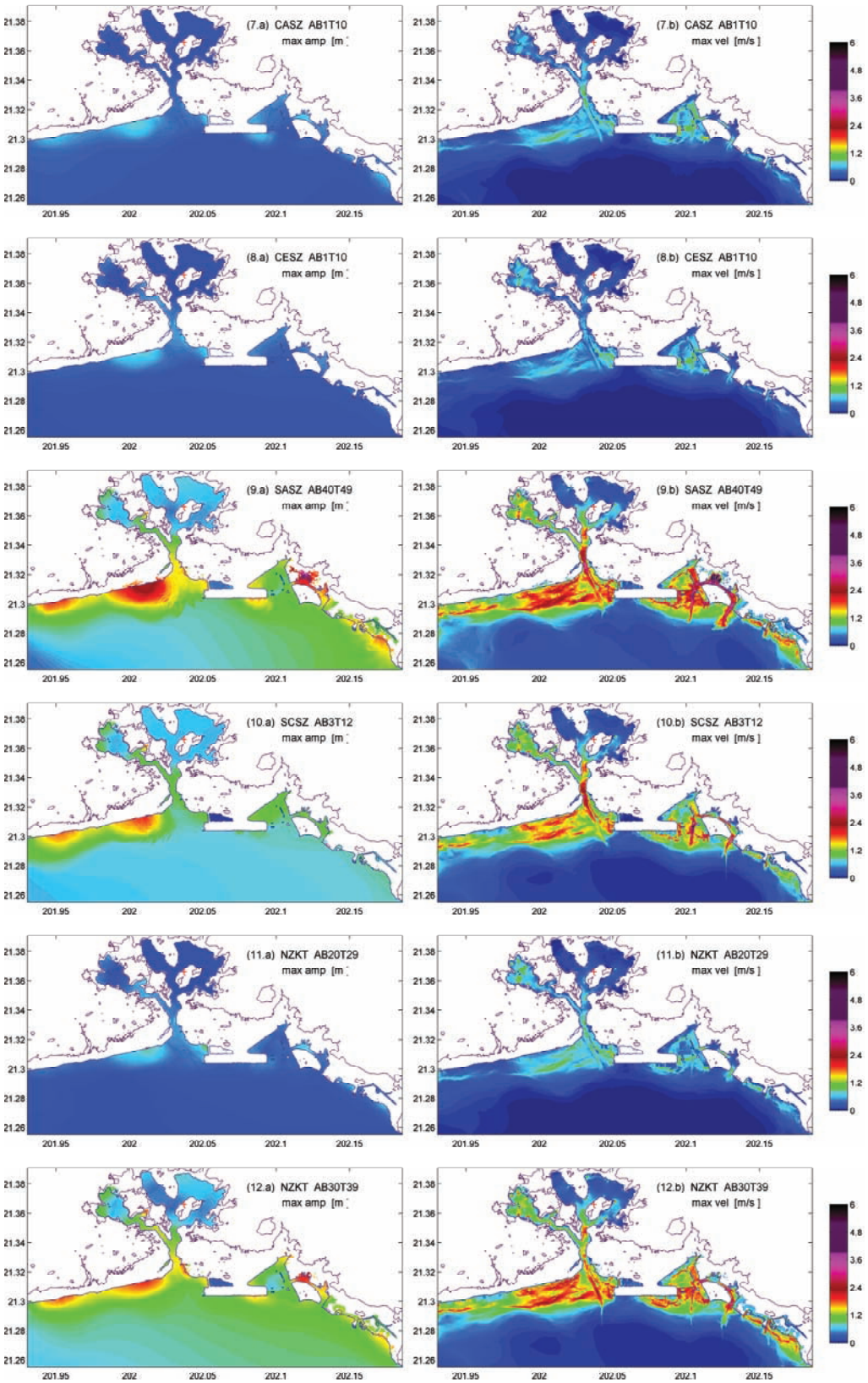

Figure A1: (continued).

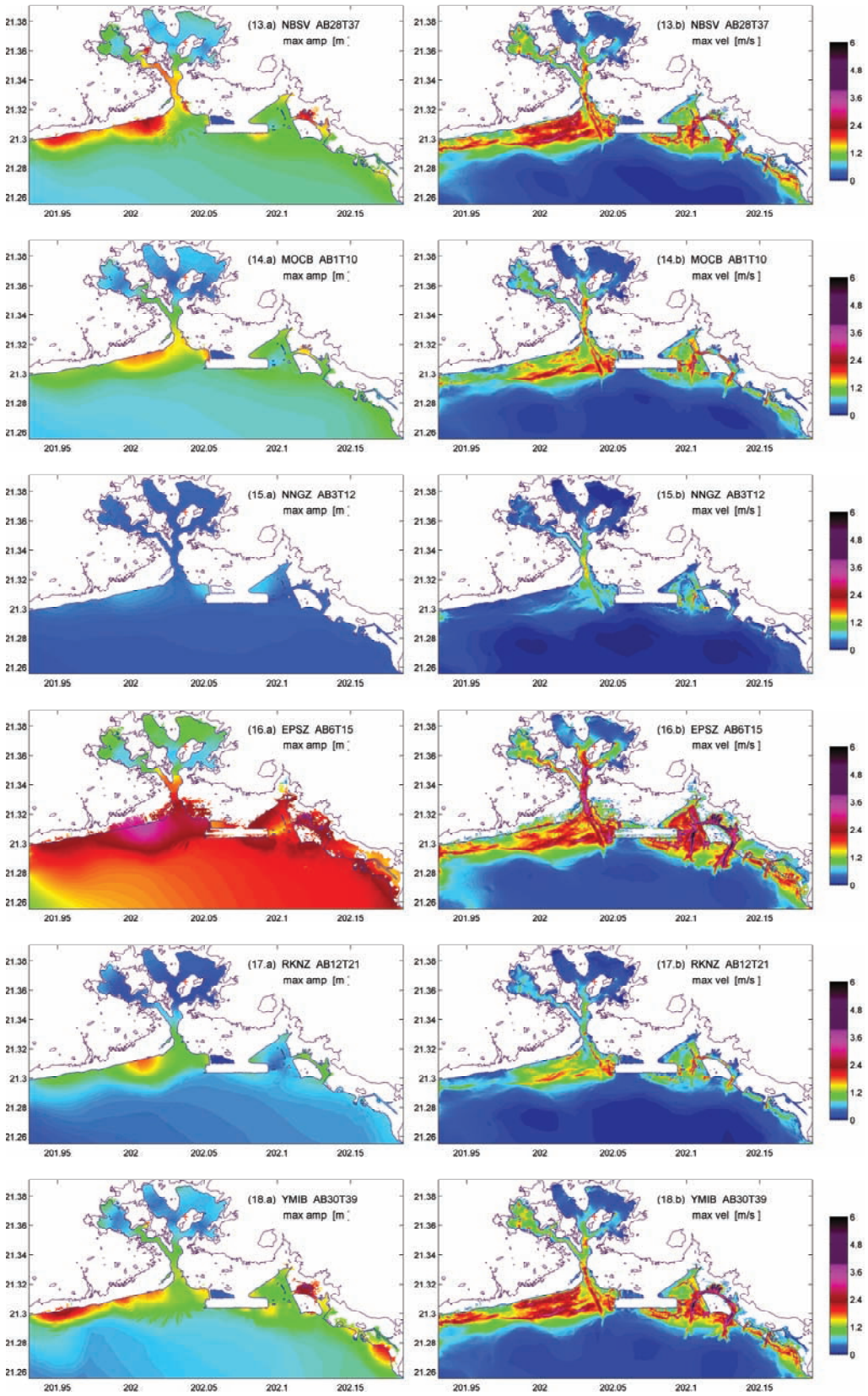

Figure A1: (continued).